https://doi.org/10.5194/egusphere-2026-6647
Preprint. Discussion started: 4 November 2026
© Author(s) 2026. CC BY 4.0 License.

Technical note: Aerosol forcing decomposition methods and recommendations

Haozhe He[1], Brian J. Soden[2], Ryan J. Kramer[3], Gabriel A. Vecchi[1,4], Jianhao Zhang[5,6], Chanyoung Park[2,7]

[1]High Meadows Environmental Institute, Princeton University, Princeton, NJ, USA
[2]Rosenstiel School of Marine, Atmospheric and Earth Science, University of Miami, Miami, FL, USA
[3]NOAA Geophysical Fluid Dynamics Laboratory, Princeton, NJ, USA
[4]Department of Geosciences, Princeton University, Princeton, NJ, USA
[5]Cooperative Institute for Research in Environmental Sciences (CIRES), University of Colorado Boulder, Boulder, CO, USA
[6]NOAA Chemical Sciences Laboratory, Boulder, CO, USA
[7]Department of Environmental Sciences, University of Virginia, Charlottesville, VA, USA

Correspondence to: Haozhe He (haozhe.he@princeton.edu)

Abstract. Aerosol effective radiative forcing (ERF), particularly its aerosol–cloud interaction component (ERF_{aci}), is commonly diagnosed using decomposition methods such as online double-call, approximate partial radiative perturbation (APRP), radiative kernels, and related proxy diagnostics. These approaches differ in whether they rely on aerosol-free or aerosol-inclusive formulations and in whether they account for cloud masking of non-cloud adjustments and, where relevant, direct aerosol effects. Here we identify a systematic bias in ERF_{aci} estimation arising from aerosol vertical structure. When aerosols reside above clouds, they attenuate incoming shortwave radiation before it reaches cloud top, thereby reducing the radiative impact of a given cloud perturbation. As a result, methods based on aerosol-free radiative sensitivities overestimate the shortwave component of ERF_{aci}, with the bias amplified in colder climate states where aerosol-over-cloud configurations are more prevalent. Thus, an apparent weakening of shortwave ERF_{aci} with warming may reflect not only a physical change in cloud response but also a reduction in aerosol-over-cloud bias as the background climate changes. In addition, neglect of cloud masking can misattribute direct aerosol effects and non-cloud adjustments. Because aerosol forcing is partitioned into direct and cloud-mediated components, this bias also affects the inferred aerosol–radiation interaction component. Simulations across multiple climate states show that diagnosed ERF partitions exhibit apparent state-dependence arising from both methodological biases and physical changes. These results highlight a broader limitation of decomposition frameworks that neglect aerosol vertical structure and cloud masking, and they underscore the need for cautious interpretation of ERF partitioning.

1 Introduction

Aerosols remain one of the largest sources of uncertainty in estimates of effective radiative forcing (ERF; Forster et al., 2021). They influence the Earth's energy balance both directly, through interactions with radiation, and indirectly, by modifying cloud properties. Following the Intergovernmental Panel on Climate Change (IPCC) framework (Boucher et al., 2013; Forster et al., 2007, 2021; Myhre et al., 2013), aerosol forcing is commonly decomposed into contributions from aerosol–radiation interactions (ERF_{ari}) and aerosol–cloud interactions (ERF_{aci}), each comprising an instantaneous radiative forcing (IRF) and subsequent rapid adjustments. This decomposition provides a useful framework for relating bulk radiative forcing to distinct physical processes.

https://doi.org/10.5194/egusphere-2026-6647
Preprint. Discussion started: 4 November 2026
© Author(s) 2026. CC BY 4.0 License.

The ERF_{ari} component arises from the scattering and absorption of radiation by aerosols, governed by their optical properties, atmospheric loading, and vertical distribution (e.g., Haywood and Boucher, 2000; Penner et al., 2001; Ramaswamy et al., 2001). It consists of IRF_{ari}, defined as the direct perturbation to top-of-atmosphere (TOA) radiative fluxes due to aerosol–radiation interactions, and rapid adjustments that are independent of surface temperature change. These adjustments include both non-cloud atmospheric responses and cloud adjustments induced by aerosol-driven changes in atmospheric thermal structure, often referred to as semi-direct effects (Hansen et al., 1997; Ackerman et al., 2000).

In contrast, ERF_{aci} reflects the influence of aerosols on cloud microphysical and macrophysical properties. Its instantaneous component, IRF_{aci}, is primarily associated with increases in cloud droplet number concentration and corresponding decreases in droplet size at fixed liquid water content, leading to enhanced cloud albedo (the Twomey effect; Twomey, 1977). This is followed by a range of rapid adjustments, whereby reduced cloud droplet size suppresses precipitation efficiency, leading to increases in liquid water content, cloud lifetime (Albrecht, 1989), and cloud thickness (Pincus and Baker, 1994). Conversely, smaller droplets can enhance entrainment mixing with surrounding dry air, thereby reducing cloud liquid condensate (e.g., Wang et al., 2003, Xue and Feingold, 2006, Bretherton et al., 2007). These adjustments can be comparable in magnitude to the instantaneous component and are sensitive to environmental conditions (Bender et al., 2019; Chen et al. 2014; Christensen et al. 2017; Ghan et al., 2016; Glassmeier et al., 2021; Gryspeerdt et al., 2017, 2019; Smith et al., 2020a; Toll et al., 2019; Zhang and Feingold, 2023). These processes remain highly uncertain, although recent assessments indicate a central estimate of ERF_{aci} of -1.0 ± 0.7 W m^{-2}, with strong agreement between observation-based and model-based estimates (Forster et al., 2021). In this technical note, ERF_{aci} is defined as the total cloud-mediated radiative response, including both traditional aerosol–cloud interactions and cloud adjustments induced by aerosol radiative heating (i.e., semi-direct effects). This definition differs slightly from the strict IPCC classification, in which semi-direct effects are formally associated with ERF_{ari}, but is adopted here for consistency with common diagnostic practice.

Despite their importance, aerosol radiative effects have historically been difficult to diagnose robustly in global climate models. Over time, coordinated modeling efforts, particularly within the Coupled Model Intercomparison Project (CMIP), have established standardized atmosphere-only experiments that enable more consistent diagnosis of aerosol ERF across models (Forster et al., 2016; Hansen et al., 2005; Pincus et al., 2016; Haywood et al., 2009; Lohmann et al., 2010). A range of diagnostic methods has been developed to partition aerosol forcing into aerosol–radiation and aerosol–cloud contributions. These include online double-call methods (Ghan, 2013), approximate partial radiative perturbation (APRP; Taylor et al., 2007; Smith et al., 2020a; Zelinka et al., 2014, 2023), radiative kernel approaches (Soden et al., 2008; Zelinka et al., 2012), and proxy diagnostics based on clear-sky fluxes and cloud radiative effect. Although these methods differ in implementation, most of them share a common feature: they diagnose the radiative impact of cloud or atmospheric changes using sensitivities or decompositions defined for a specified background state. In many practical applications, these diagnostics do not explicitly account for interactions between aerosol vertical structure and cloud radiative responses.

https://doi.org/10.5194/egusphere-2026-6647
Preprint. Discussion started: 4 November 2026
© Author(s) 2026. CC BY 4.0 License.

This limitation may become important across different climate states or aerosol configurations. When aerosols are located above clouds, they attenuate incoming shortwave radiation before it reaches cloud top. Under such conditions, the radiative effect of a given cloud perturbation is smaller than would be inferred from an aerosol-free kernel or related diagnostic (Figs. 1a–c); methods that neglect this attenuation therefore overestimate the shortwave cloud radiative response and thus bias estimates of ERF_{aci}. Because the prevalence and radiative importance of aerosol-over-cloud configurations can vary with the background climate, the magnitude of this attenuation and the resulting diagnostic bias may also differ across climate states, introducing apparent state-dependence in diagnosed forcing components.

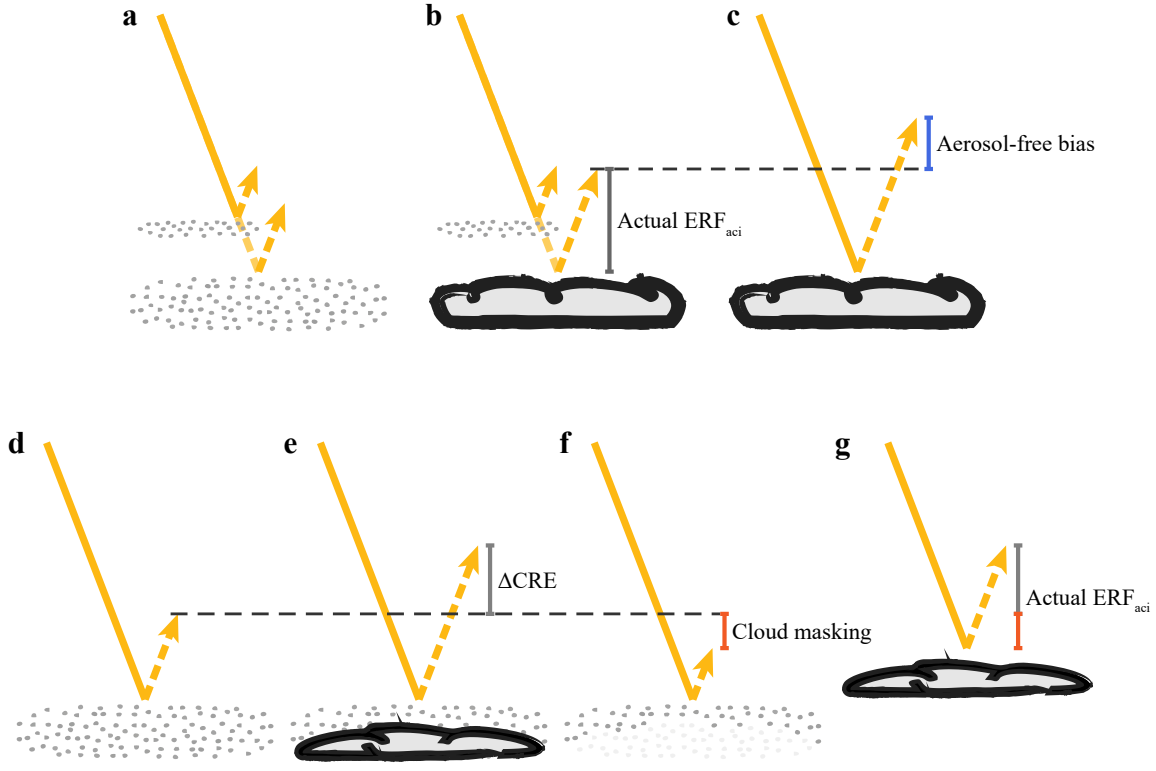


Figure 1: Schematic illustration of how aerosols above clouds and cloud masking affect estimates of ERF_{aci} in an aerosol-only perturbation experiment with fixed SST, thereby excluding surface-temperature-mediated responses. (a–c) Idealized vertical structures (a) and the corresponding ERF_{aci} diagnosed using aerosol-inclusive (b) and aerosol-free (c) methods, with the aerosol radiative effect in (a) shown under clear-sky conditions. (d–g) Idealized aerosol distributions (d) and the associated decomposition of ERF_{aci} (g) into ΔCRE (e) and cloud-masking contributions (f); panel (d) shows the clear-sky aerosol radiative effect before cloud masking. Particular emphasis is placed on the masking of direct aerosol effects and non-cloud atmospheric adjustments. Arrows and bars are for illustrative purposes and are not plotted to scale.

In this technical note, we examine this methodological issue. We first summarize commonly used aerosol forcing decomposition methods and their underlying assumptions, with particular attention to aerosol vertical structure and cloud-masking effects. We then demonstrate how aerosol-over-cloud geometry biases ERF_{aci} estimates and how this bias varies with climate state. Finally, using simulations across a range of imposed base-state climates, we show that diagnosed ERF

https://doi.org/10.5194/egusphere-2026-6647
Preprint. Discussion started: 4 November 2026
© Author(s) 2026. CC BY 4.0 License.

partitions reflect both methodological biases and genuine physical changes. Our goal is not to replace existing methods, but to clarify their interpretation and provide guidance for their application.

2. Overview of common decomposition methods and their implicit assumptions

Building on these standardized atmosphere-only experiments, in which sea surface temperature (SST) and sea ice are prescribed, aerosol ERF is often further decomposed into physically interpretable components using a small number of established diagnostic frameworks. Here, for clarity, we discuss these methods in the context of aerosol-only perturbation experiments with fixed SST, thereby avoiding complications from surface temperature mediated changes and their associated radiative feedbacks. It should be noted, however, that fixed-SST simulations still permit some land surface temperature changes; although these responses are usually small for aerosol forcing, they are not strictly negligible. Because this technical note focuses on the interpretation of these diagnostics rather than on a full methodological derivation, we summarize only their key features and the aspects most relevant to aerosol vertical structure and cloud-masking effects.

Our discussion focuses primarily on the diagnosis of IRF_{ari} and ERF_{aci}. We focus on IRF_{ari}, rather than total ERF_{ari}, for two reasons. First, non-cloud atmospheric rapid adjustments are diagnosed separately using the radiative kernel framework (Soden et al., 2008), which is the primary available method for estimating these adjustments, especially under all-sky conditions. Second, we do not attempt to isolate the semi-direct effect from the total cloud radiative response. Accordingly, ERF_{aci} is interpreted as the total cloud-mediated radiative response, consistent with the definition adopted in the Introduction.

A useful way to organize the available methods is to begin with the radiative flux quantities from which many decompositions are constructed, namely clear-sky and all-sky TOA radiative flux changes and the associated cloud radiative effect (CRE), and then consider the more formal diagnostic frameworks built on them. Here, CRE is defined as the difference between all-sky and clear-sky radiative fluxes.

2.1 Cloud radiative effect and clear-sky flux changes

For aerosol-only perturbation experiments with fixed SST, the simplest diagnostics of aerosol forcing are based on changes in all-sky and clear-sky radiative fluxes at the TOA, together with the associated change in CRE (ΔCRE). In this approach, ΔCRE is often used as a proxy for aerosol–cloud interactions (e.g., Chen et al., 2010; Gettelman et al., 2012; Hoose et al., 2009; Rotstayn and Liu, 2005; Rotstayn and Penner, 2001), under the assumption that variations in cloud radiative impact primarily reflect aerosol-induced cloud changes. The corresponding clear-sky flux change is then often interpreted as a proxy for aerosol–radiation interactions, because it excludes the direct radiative effects of clouds. These diagnostics are straightforward and can be obtained directly from standard model output, making them attractive for intercomparison and exploratory analysis.

https://doi.org/10.5194/egusphere-2026-6647
Preprint. Discussion started: 4 November 2026
© Author(s) 2026. CC BY 4.0 License.



However, such proxy diagnostics do not provide a clean physical partition. ΔCRE can reflect not only aerosol-induced cloud changes, but also cloud masking of non-cloud atmospheric perturbations and, where relevant, direct aerosol effects (Soden et al., 2008; Figs. 1d–g). In addition, interpreting ΔCRE as aerosol–cloud forcing implicitly assigns the clear-sky forcing to the direct aerosol term. Ghan (2013) showed that this partition is biased because the inferred direct term reduces to a clear-sky estimate, which does not properly account for the radiative effects of aerosol located above clouds. In such cases, absorbing and scattering aerosol above clouds modify the all-sky direct effect through cloud masking, so the partition misattributes part of that signal to the cloud-mediated term. From the perspective of the present study, the same aerosol-over-cloud geometry also reduces the shortwave radiation reaching cloud top, thereby weakening the radiative sensitivity of cloud perturbations. Consequently, neither ΔCRE nor clear-sky flux anomalies provide a unique isolation of aerosol-cloud and aerosol–radiation interactions. These limitations are particularly important in the present context, because aerosol vertical structure, background climate state, and cloud masking can all affect how clear-sky and all-sky flux anomalies are interpreted.

2.2 Radiative kernel method

Radiative kernels provide a flexible framework for decomposing ERF into contributions from different physical processes by relating radiative perturbations associated with rapid adjustments to changes in atmospheric variables through precomputed radiative sensitivities (Soden et al., 2008). In aerosol forcing studies, they are particularly valuable because they provide the primary method for separating non-cloud atmospheric adjustment terms, including contributions from temperature, water vapor, and surface albedo changes, from the total radiative forcing, especially under all-sky conditions.

In fixed-SST simulations, the TOA energy imbalance, ΔN, which is equivalent here to ERF, can be expressed as the sum of IRF_{ari} and the radiative response associated with rapid adjustments, ΔR:

$$ERF = \Delta N = IRF_{ari} + \Delta R, \quad (1)$$

To first order, the radiative response can be decomposed into contributions from temperature (T), water vapor (q), surface albedo (α), and clouds (Cld):

$$\Delta R = \Delta R_T + \Delta R_q + \Delta R_\alpha + \Delta R_{Cld}, \quad (2)$$

Following Soden et al. (2008), the non-cloud radiative responses are estimated directly with radiative kernels. For a given variable x, the adjustment can be written in linear form as

$$\Delta R_x = K_x \Delta x, \quad (3)$$

where K_x is the radiative kernel, representing the radiative sensitivity to perturbations in x, i.e., $K_x = \partial R/\partial x$, and Δx is the simulated change in that variable; in practice, x typically represents temperature, water vapor, or surface albedo. In this work, we use the radiative kernels developed by Smith et al. (2020b), which are based on the atmospheric component of a recent-generation climate model, HadGEM3, from the UK Met Office.

Under clear-sky conditions, the same decomposition can be written as

$$ERF^{clr} = \Delta N^{clr} = IRF_{ari}^{clr} + \Delta R^{clr}, \quad (4)$$

https://doi.org/10.5194/egusphere-2026-6647
Preprint. Discussion started: 4 November 2026
© Author(s) 2026. CC BY 4.0 License.

where the superscript "clr" denotes clear-sky conditions, and

$$\Delta R^{clr} = \Delta R_T^{clr} + \Delta R_q^{clr} + \Delta R_\alpha^{clr}, \quad (5)$$

This allows clear-sky IRF_{ari} to be diagnosed directly as

$$IRF_{ari}^{clr} = ERF^{clr} - \Delta R^{clr} = \Delta N^{clr} - \left(\Delta R_T^{clr} + \Delta R_q^{clr} + \Delta R_\alpha^{clr}\right), \quad (6)$$

The cloud radiative response, ΔR_{Cld}, which we denote here as ERF_{aci}, cannot be diagnosed directly under all-sky conditions because cloud effects are embedded in the difference between all-sky and clear-sky radiative perturbations. In the traditional radiative kernel framework, ERF_{aci} is therefore estimated from ΔCRE after correction for cloud masking (Soden et al., 2004, 2008):

$$ERF_{aci} = \Delta R_{Cld} = \Delta CRE - (\Delta R_T - \Delta R_T^{clr}) - \left(\Delta R_q - \Delta R_q^{clr}\right) - (\Delta R_\alpha - \Delta R_\alpha^{clr}) - \left(IRF_{ari} - IRF_{ari}^{clr}\right), \quad (7)$$

Here, the cloud-masking correction accounts for the fact that ΔCRE contains not only the radiative response to cloud changes, but also the all-sky minus clear-sky differences in non-cloud adjustments and IRF_{ari}. In other words, part of what appears in ΔCRE reflects the masking of non-cloud radiative perturbations by clouds rather than a true cloud radiative response. This distinction is central to the present study, because cloud masking also complicates the interpretation of aerosol-forcing partitions when aerosol vertical structure matters.

Unlike the clear-sky case, all-sky IRF_{ari} cannot be diagnosed directly from the residual because estimating ΔR_{Cld} itself requires knowledge of IRF_{ari}. Following common practice (Soden et al., 2008; Vial et al., 2013), we therefore estimate all-sky IRF_{ari} from the clear-sky value using a cloud-masking factor:

$$IRF_{ari} = IRF_{ari}^{clr}/Cl, \quad (8)$$

where Cl is a constant representing the cloud masking of IRF_{ari}.

For longwave forcing, we use a cloud-masking factor of 1.24, derived from the ratio of clear-sky to all-sky double-call radiative transfer estimates of CO_2 IRF in the Precipitation Driver and Response Model Intercomparison Project (PDRMIP; Myhre et al., 2016; Smith et al., 2018). For shortwave aerosol forcing, we adopt a global-mean cloud-masking factor of 2.43 following Kramer et al. (2021), derived from direct aerosol IRF output from MERRA-2 (Gelaro et al., 2017) and consistent with the observationally constrained range summarized by Bellouin et al. (2020).

The key assumption underlying the radiative kernel framework is that radiative sensitivities are evaluated about a specified background state and can be applied linearly to the perturbation of interest. This approximation is often reasonable for diagnosing rapid adjustments within the fixed-SST configurations, but becomes more uncertain when the effective radiative sensitivities of the simulated perturbations differ substantially from those of the state in which the kernels were derived (Jonko et al., 2012). This issue is especially relevant here because cloud masking, aerosol vertical structure, and background climate state can all influence the effective radiative sensitivity of aerosol-induced perturbations.

https://doi.org/10.5194/egusphere-2026-6647
Preprint. Discussion started: 4 November 2026
© Author(s) 2026. CC BY 4.0 License.

2.3 Approximate partial radiative perturbation technique

APRP is a shortwave decomposition method based on a simplified one-layer representation of shortwave radiative transfer (Taylor et al., 2007). Because it relies only on standard radiative flux output and does not require additional radiation calls, it is computationally efficient and has been widely used in model intercomparison studies to decompose shortwave aerosol forcing into contributions from different physical processes (e.g., Smith et al., 2020a; Zelinka et al., 2023). Using clear-sky and all-sky shortwave fluxes at the TOA and surface, together with cloud fraction, APRP diagnoses effective atmospheric scattering and absorption parameters and uses the resulting sensitivities of planetary albedo to attribute shortwave radiative changes to perturbations in surface albedo, clouds, and non-cloud atmospheric constituents, which in this case include water vapor and aerosols. In this sense, APRP provides an efficient approximation to the more rigorous but more difficult-to-implement partial radiative perturbation (PRP) technique. Taylor et al. (2007) showed that APRP reproduces PRP-derived shortwave cloud and surface-albedo radiative responses reasonably well, with errors generally smaller than about 10 %. In this study, APRP is used to diagnose shortwave direct forcing and adjustment metrics.

Because the non-cloud atmospheric contribution diagnosed by APRP includes both water vapor and aerosols, shortwave IRF_{ari} is estimated by subtracting the water vapor adjustment diagnosed using radiative kernels from this contribution, even though shortwave water vapor absorption is generally small. Since APRP is limited to shortwave radiation, longwave contributions in this work are diagnosed using radiative kernels under analogous aerosol-inclusive conditions, so the total estimate combines APRP-based shortwave terms with kernel-based longwave terms. For brevity, we refer to this hybrid approach as APRP+kernels. Despite the advantages noted above, APRP remains an approximate framework. It does not explicitly resolve the full three-dimensional coupling among aerosol vertical structure, cloud perturbations, and radiative transfer. As a result, although it is useful for diagnosing broad shortwave contributions, differences from more direct estimates may arise, particularly under aerosol-over-cloud conditions.

2.4 Online double-call method

Double-call radiative transfer calculations provide one of the most direct methods for diagnosing IRF in model simulations. In this framework, an additional diagnostic call to the radiation scheme is performed at each time step using the same atmospheric state but with a prescribed perturbation to the forcing agent. For aerosol applications, this typically involves neglecting aerosol scattering and absorption, thereby isolating the aerosol radiative perturbation within the model's native radiation code. These calculations are used only for diagnostic purposes and do not feed back onto the simulated climate state. Because they are carried out online within the radiation code, the double-call method avoids some of the approximations inherent in offline decomposition approaches while providing a relatively direct estimate of aerosol forcing components.

A widely used implementation of this approach is the aerosol-free radiative decomposition introduced by Ghan (2013). In this framework, the model archives the standard all-sky and clear-sky radiative fluxes, F and F^{clr}, together with their aerosol-

https://doi.org/10.5194/egusphere-2026-6647
Preprint. Discussion started: 4 November 2026
© Author(s) 2026. CC BY 4.0 License.

free counterparts from the additional diagnostic radiation call, F^{af} and $F^{clr,\,af}$, where the superscript 'af' indicates that aerosol scattering and absorption are neglected. In the notation of Ghan (2013), the total aerosol forcing can then be decomposed as

$$ERF = \Delta F = \Delta(F - F^{af}) + \Delta(F^{af} - F^{clr,af}) + \Delta F^{clr,af}, \quad (9)$$

where the first term represents the direct aerosol radiative forcing (IRF_{ari}), the second term the cloud-mediated forcing (ERF_{aci}), and the third term is primarily associated with aerosol-induced changes in surface albedo. Because this third term is defined under clear-sky conditions, it can also include contributions from non-cloud adjustments that are not naturally assigned to either the direct aerosol or cloud-mediated components (Zelinka et al., 2023). In this framework, the ERF_{aci} term can also be interpreted as ΔCRE^{af}, which provides a useful point of comparison with other decomposition methods.

This framework has been widely used because, by diagnosing forcing components directly within the online radiation code, it yields terms that are more closely tied to the underlying radiative processes than simpler ΔCRE and clear-sky flux changes, while leaving the total aerosol forcing unchanged. It has also been extended to partition aerosol–cloud interactions into contributions associated with cloud droplet number, liquid water path, and cloud fraction adjustments (e.g., Gryspeerdt et al., 2020).

However, aerosol-free radiative calculations still rely on assumptions that are important in the present context. In particular, by diagnosing cloud-mediated radiative effects under aerosol-free conditions, they implicitly assume that the radiative sensitivity to cloud changes is unaffected by aerosol vertical structure. When aerosols are located above clouds, this assumption can break down. In such cases, overlying aerosol reduces the shortwave radiation reaching cloud top, so the actual radiative impact of a given cloud perturbation differs from that inferred under aerosol-free conditions. Consequently, even online double-call methods can complicate the interpretation of the partition between direct and cloud-mediated forcing when aerosol-over-cloud geometry is important.

2.5 Cloud radiative kernel method

Another common approach for diagnosing ERF_{aci} is the cloud radiative kernel method, in which cloud changes are represented as functions of cloud-top pressure and optical depth, and then combined with precomputed radiative sensitivities to estimate the cloud radiative response. In practice, this is often implemented using satellite-simulator output, most commonly from the ISCCP (International Satellite Cloud Climatology Project) simulator and, when available, from the MODIS (Moderate Resolution Imaging Spectroradiometer) simulator. For example, the ISCCP simulator provides a joint 7 × 7 histogram of cloud visible optical depth and cloud-top pressure (Klein and Jakob, 1999; Webb et al., 2001), which can be combined with the corresponding simulator kernel to estimate the associated shortwave and longwave TOA radiative effects (Zelinka et al., 2012). This approach links changes in cloud properties directly to their radiative effects, providing a compact and physically interpretable estimate of cloud-mediated forcing that is readily applicable across models.

In contrast to ΔCRE-based approaches, the cloud radiative kernel method does not infer the cloud radiative response from all-sky and clear-sky flux differences and therefore does not require the same explicit correction for cloud masking of non-

https://doi.org/10.5194/egusphere-2026-6647
Preprint. Discussion started: 4 November 2026
© Author(s) 2026. CC BY 4.0 License.

cloud adjustments. It has also been shown to agree well with cloud feedback estimates derived from radiative kernel methods (Zelinka et al., 2012; He et al., 2024), which account for cloud masking of non-cloud adjustments. This agreement is consistent with the cloud radiative kernel method capturing the corresponding cloud radiative response without requiring these adjustments to be explicitly subtracted. However, cloud radiative kernels are generally developed for cloud feedback calculations and are most commonly derived from offline radiative-transfer calculations under aerosol-free conditions (Zelinka et al., 2012). Applying these kernels to ERF_{aci} therefore implicitly assumes that the amount of incident shortwave radiation reaching the cloud layer is unaffected by aerosol perturbations above cloud top. As in the double-call framework discussed above, this assumption can fail under aerosol-over-cloud conditions, where overlying aerosol reduces the shortwave radiation reaching the cloud layer. As a result, the actual shortwave radiative impact of a given cloud perturbation is smaller than that predicted by the aerosol-free kernel, so diagnosed shortwave ERF_{aci} can be biased toward more negative values.

2.6 Relevance to this note

The methods summarized above provide complementary perspectives on aerosol forcing decomposition and differ in their assumptions, required diagnostics, and sources of uncertainty. These methodological characteristics, including the treatment of aerosol radiative effects, cloud masking, and the main diagnosed components, are summarized in Table 1. None is inherently invalid. The point emphasized in this technical note is more specific: the interpretation of these decompositions depends critically on how they treat aerosol vertical structure, which affects the radiative sensitivity of cloud perturbations, and on whether they account for the cloud-masking effects of non-cloud adjustments and direct aerosol forcing.

Table 1. Characteristics summary of aerosol-forcing decomposition methods considered in this study.

Method	Aerosol treatment for ERF_{aci}	Treatment of cloud masking	Main diagnosed components
ΔCRE / clear-sky flux change	**Aerosol-inclusive**: uses standard aerosol-containing all-sky and clear-sky radiative fluxes	**Not explicitly corrected**. ΔCRE contains cloud masking of non-cloud adjustments and direct aerosol effects	**SW + LW**: ΔCRE as a proxy for ERF_{aci}; clear-sky flux change as a proxy for IRF_{ari}
Radiative kernels	**Aerosol-inclusive**: uses standard aerosol-containing all-sky and clear-sky radiative fluxes together with precomputed kernels applied to simulated temperature, water vapor, and surface albedo changes	**Explicitly corrected** for cloud masking of non-cloud adjustments and direct aerosol forcing (IRF_{ari}); all-sky IRF_{ari} requires an assumed cloud-masking factor	**SW + LW**: ERF_{aci}, IRF_{ari}, and non-cloud adjustments from temperature, water vapor, and surface albedo
APRP	**Aerosol-inclusive**: uses standard aerosol-	**No conventional cloud-**	**SW only***: SW ERF_{aci}, including

https://doi.org/10.5194/egusphere-2026-6647
Preprint. Discussion started: 4 November 2026
© Author(s) 2026. CC BY 4.0 License.

	containing all-sky and clear-sky SW fluxes at the TOA and surface, together with cloud fraction	**masking correction required**. The cloud contribution is diagnosed directly from its contribution to the change in planetary albedo rather than inferred from ΔCRE	cloud amount, scattering, and absorption contributions; non-cloud atmospheric contribution; and surface albedo contribution. SW IRF_{ari} is obtained from the non-cloud atmospheric contribution after subtracting the water vapor adjustment
Online double-call	**Aerosol-free for ERF_{aci}**: uses aerosol-free ΔCRE (ΔCRE^{af}), calculated from aerosol-free all-sky and clear-sky radiative fluxes obtained from an additional online radiation call; attenuation of shortwave radiation by aerosol above cloud is not represented	**Not explicitly corrected**. ΔCRE^{af} retains cloud masking of non-cloud adjustments, while cloud masking of direct aerosol forcing is absent by construction	**SW + LW**: ERF_{aci} and IRF_{ari}, plus an aerosol-free clear-sky term primarily associated with surface albedo and other non-cloud adjustments
Cloud radiative kernels	**Aerosol-free for ERF_{aci}**: uses cloud-simulator output combined with precomputed cloud radiative kernels, most commonly derived from radiative-transfer calculations without aerosol radiative effects; attenuation of shortwave radiation by aerosol above cloud is not represented	**No conventional ΔCRE cloud-masking correction required**. Cloud-property changes are mapped directly to radiative effects. This approach has been shown to agree well with cloud feedback estimates derived using radiative kernels that explicitly account for cloud masking	**SW + LW**: ERF_{aci}, including contributions from changes in cloud amount, optical depth/scattering, and cloud altitude

*: SW only, but radiative kernels are used for LW components and the SW water vapor adjustment in this study.

In particular, methods formulated under aerosol-free conditions, or methods that do not explicitly account for cloud masking of non-cloud atmospheric adjustments and, especially, direct aerosol effects, can misattribute forcing when aerosol vertical structure is important. This issue is especially consequential when aerosols reside above clouds, because aerosol-over-cloud geometry reduces the effective shortwave radiative sensitivity of cloud perturbations relative to that implied by aerosol-free conditions. This effect is related to, but distinct from, traditional cloud masking in clear-sky versus all-sky decompositions, because it reflects a change in the effective radiative sensitivity of cloud perturbations themselves rather than only the masking of non-cloud radiative terms by clouds.

https://doi.org/10.5194/egusphere-2026-6647
Preprint. Discussion started: 4 November 2026
© Author(s) 2026. CC BY 4.0 License.

Consequently, aerosol-over-cloud geometry can bias the diagnosed shortwave ERF_{aci} high and can also affect the inferred partition between direct and cloud-mediated forcing. The central methodological concern here is therefore not that any one decomposition framework is universally incorrect, but that many practical implementations assume that the radiative effect of a cloud perturbation can be evaluated independently of aerosol vertical structure. That assumption can break down under aerosol-over-cloud conditions and, as shown later, can contribute to the apparent state-dependence of diagnosed aerosol forcing components.

3 State-dependence of diagnosed forcing components

Because each of the decomposition methods discussed above relies on its own set of assumptions, evaluation within a single base-state provides only a limited assessment of method behavior. Here, we assess these decomposition frameworks across a broad range of base-state climates, allowing their state-dependence and associated methodological biases to be examined explicitly.

The cloud background state varies systematically with climate. As climate warms, increased atmospheric moisture generally favors optically thicker clouds and greater cloud liquid water, whereas colder climates, particularly at high latitudes, tend to have thinner or less liquid-rich clouds (Fig. A1). These differences influence both aerosol–cloud overlap and the radiative sensitivity of cloud perturbations. In colder climates, aerosols are more likely to reside above rather than within the cloud layer, increasing the prevalence of aerosol-over-cloud configurations. This pattern may partly reflect relatively limited cloud processing and precipitation removal in colder climates, where the availability of liquid water is lower (He et al., 2026). As a result, attenuation of incoming shortwave radiation by overlying aerosol has a larger relative effect on the radiative sensitivity of cloud changes. Consequently, the aerosol-over-cloud bias is not expected to remain constant across climate states. Decomposition frameworks based on aerosol-free radiative sensitivities can therefore spuriously introduce or amplify apparent trends in ERF partitions across climate states. An apparent weakening of shortwave ERF_{aci} with warming may thus reflect not only a genuine physical change in cloud response, but also a reduction in the bias associated with aerosol-over-cloud geometry as the background climate changes.

3.1 Experimental framework

To examine how these decomposition methods behave across climate states, we analyze a set of atmosphere-only simulations performed with GFDL-AM4.0 (Zhao et al., 2018a, b) and GFDL-AM4-MG2 (Guo et al., 2021) under prescribed SST and sea-ice boundary conditions on the Princeton University Tiger2 supercomputer. GFDL-AM4.0 is the standard atmospheric model configuration, whereas GFDL-AM4-MG2 implements the two-moment Morrison–Gettelman bulk cloud microphysics scheme with prognostic precipitation (Gettelman and Morrison, 2015), together with a mineral-dust- and temperature-dependent ice-nucleation scheme (Fan et al., 2019). These simulations were originally developed to investigate the state-dependence of cloud feedback (He et al., 2024). A present-day reference simulation (0K) is integrated for 30 years

https://doi.org/10.5194/egusphere-2026-6647
Preprint. Discussion started: 4 November 2026
© Author(s) 2026. CC BY 4.0 License.

using monthly climatological SST and sea ice for 1986–2005, with radiatively active gas concentrations and aerosol emissions fixed at corresponding present-day values representative of 1990s conditions. The atmosphere is free-running, without wind nudging. Additional experiments are then performed with uniform SST perturbations of −8 K, −4 K, +4 K, and +8 K, denoted m8K, m4K, p4K, and p8K, respectively. For each base-state climate, a corresponding simulation is conducted with preindustrial aerosol emissions under otherwise identical boundary conditions and forcings, with the present-day aerosol case treated as the perturbed experiment and the preindustrial aerosol case as the control experiment. This design allows aerosol forcing to be diagnosed separately within each base-state climate as the difference between the present-day and preindustrial aerosol cases, thereby making its dependence on background climate explicit.

The differences between the two model configurations are not the primary focus of this technical note, although their distinct cloud microphysics provide useful context for interpreting the results. Instead, the use of two distinct models provides a broader basis for evaluating the decomposition methods across different background cloud states and aerosol–cloud configurations. Our emphasis here is therefore not on the full physical interpretation of state-dependent aerosol forcing, which is addressed in a parallel study, but on how different decomposition methods behave across this range of base-state climates.

3.2 Estimates of ERF_{aci} across methods

Figure 2 compares the diagnosed ERF_{aci} across decomposition methods for the five base-state climates in GFDL-AM4.0 and GFDL-AM4-MG2. Aerosol-free estimates (undotted bars in Fig. 2) from the online double-call and cloud radiative kernel methods are shown together with aerosol-inclusive estimates (dotted bars in Fig. 2) from the APRP+kernels, radiative kernel, and CRE proxy methods, allowing the influence of aerosol-over-cloud treatment on the diagnosed forcing to be assessed directly.

https://doi.org/10.5194/egusphere-2026-6647
Preprint. Discussion started: 4 November 2026
© Author(s) 2026. CC BY 4.0 License.

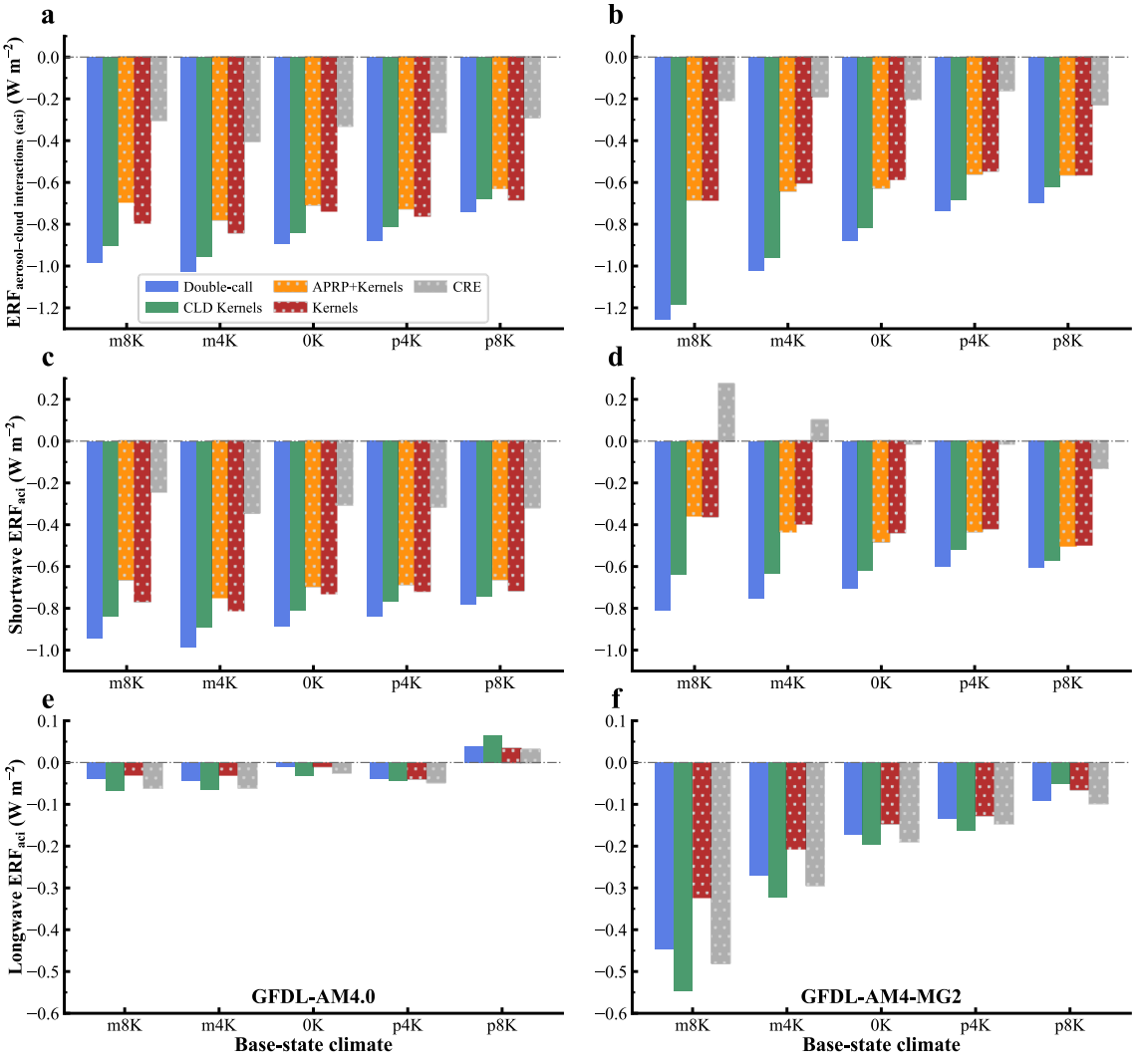


Figure 2: Total, shortwave, and longwave ERF_{aci} diagnosed using different decomposition methods across the five base-state climates. Rows from top to bottom show total, shortwave, and longwave results, respectively. The left column shows GFDL-AM4.0 and the right column shows GFDL-AM4-MG2. For each climate state, bars without overlaid dots indicate estimates from aerosol-free decomposition methods, whereas bars with overlaid dots indicate estimates from aerosol-inclusive methods. The vertical axis range in the bottom row is half that used in the top and middle rows.

A clear feature of the figure is that aerosol-free methods generally diagnose a stronger negative ERF_{aci} than aerosol-inclusive methods. This discrepancy is dominated by the shortwave component, where the separation between aerosol-free and aerosol-inclusive estimates is systematically largest. The behavior is consistent with the mechanism discussed above: when aerosols reside above cloud top, aerosol-free methods evaluate cloud perturbations using a shortwave radiative sensitivity that is too large because attenuation of incoming solar radiation by overlying aerosol is neglected. As a result, the shortwave radiative impact of a given cloud change is overestimated, yielding a more negative diagnosed shortwave ERF_{aci}.

https://doi.org/10.5194/egusphere-2026-6647
Preprint. Discussion started: 4 November 2026
© Author(s) 2026. CC BY 4.0 License.

The state-dependence of this bias is also evident in Fig. 2. In both models, the discrepancy between aerosol-free and aerosol-inclusive estimates is generally larger in the colder base-states and smaller in the warmer ones. This pattern is particularly clear in the shortwave panels and is consistent with the expectation that colder climates, especially at higher latitudes, favor thinner or less liquid-rich clouds, increasing the prevalence of aerosol-over-cloud configurations (Fig. A1). This state-dependence emerges even though the imposed aerosol perturbation is held fixed across the base-states. Under these conditions, aerosol-over-cloud attenuation has a larger relative effect on the radiative sensitivity of cloud changes, so the bias in aerosol-free ERF_{aci} estimates becomes larger. In warmer states, aerosol-free estimates move closer to aerosol-inclusive estimates, especially for the APRP and radiative kernel methods, consistent with a reduction in aerosol-over-cloud bias. Taken together, these results support the use of aerosol-inclusive methods for diagnosing ERF_{aci}, since their estimates are less sensitive to the aerosol-over-cloud bias that affects aerosol-free decompositions.

Differences among the aerosol-inclusive methods further clarify the role of cloud masking. The larger discrepancy between the aerosol-inclusive APRP or radiative kernel estimates and ΔCRE indicates that cloud masking of non-cloud adjustments and direct aerosol effects remains a substantial contributor even when aerosol-over-cloud attenuation is explicitly accounted for. In fixed-SST configurations, aerosol forcing inevitably induces mild land cooling, accompanied by reduced atmospheric water vapor and, in some regions, increased surface albedo. These non-cloud adjustments contribute to the difference between ΔCRE and ERF_{aci} through cloud masking. In particular, increased surface albedo produces a negative shortwave albedo adjustment, and partial masking of this adjustment by clouds contributes to a more negative ERF_{aci} relative to ΔCRE. The shortwave water vapor adjustment is comparatively small and therefore likely contributes less. More importantly, cloud masking of direct aerosol effects can be substantial, especially in the shortwave (Figs. 1d–g). Taken together, these contributions make ERF_{aci} more negative than would be inferred from ΔCRE alone. In this light, the positive shortwave ΔCRE diagnosed in GFDL-AM4-MG2 is difficult to interpret as ERF_{aci}, which is generally expected to represent a cooling effect in the shortwave. More broadly, this comparison highlights the importance of accounting for both aerosol vertical structure and cloud masking when estimating ERF_{aci}.

Within the aerosol-free category, the methods also differ in informative ways. As discussed in Section 2.4, the ERF_{aci} term from the online double-call framework can be interpreted as ΔCRE^{af}. By contrast, the aerosol-free cloud radiative kernel estimate appears to account for the masking of non-cloud adjustments under aerosol-free conditions, consistent with the agreement between cloud feedback estimates derived from cloud radiative kernel and radiative kernel methods (Zelinka et al., 2012; He et al., 2024). For comparison, the relationship between these diagnostics can be expressed as:

$$ERF_{aci} = \Delta CRE^{af} - \left(\Delta R_T^{af} - \Delta R_T^{clr,af}\right) - \left(\Delta R_q^{af} - \Delta R_q^{clr,af}\right) - \left(\Delta R_\alpha^{af} - \Delta R_\alpha^{clr,af}\right), \quad (10)$$

However, the shortwave ERF_{aci} from the aerosol-free cloud radiative kernel method is systematically less negative than that from the online double-call decomposition across base-states and in both models, a feature also evident in Smith et al. (2020, their Fig. 11). Interpreted literally, this would imply a positive contribution from cloud masking of shortwave water vapor and surface albedo adjustments, with magnitudes ranging from 0.04 to 0.11 W m^{-2} in GFDL-AM4.0 and from 0.03 to 0.17

https://doi.org/10.5194/egusphere-2026-6647
Preprint. Discussion started: 4 November 2026
© Author(s) 2026. CC BY 4.0 License.

W m^{-2} in GFDL-AM4-MG2, thereby making the cloud radiative kernel estimate less negative than ΔCRE^{af}. From a physical standpoint, however, one might expect the cloud-masking contributions from non-cloud adjustments to become more negative under aerosol-free conditions, because removing aerosol attenuation increases the shortwave radiation reaching the cloud layer. The fact that the aerosol-free cloud radiative kernel estimates instead show the opposite tendency makes their behavior difficult to interpret and suggests that the treatment of cloud masking in this framework is not straightforward. For the purposes of this technical note, the main point is that even within the aerosol-free category, the diagnosed ERF_{aci} depends sensitively on how cloud masking and aerosol-free radiative sensitivities are treated.

By contrast, the longwave component shows much smaller differences across methods, especially noting that the vertical axis range in the bottom row is only half that used in the top and middle rows. This indicates that the main methodological discrepancy arises in the shortwave term rather than in the longwave cloud response itself, which is physically expected because the aerosol-over-cloud mechanism primarily affects incoming shortwave radiation. Even so, some longwave differences remain worth noting. Longwave ΔCRE is consistently and modestly more negative than ΔCRE^{af} across base-states and in both models, except for the warmest base-state in GFDL-AM4.0, where ΔCRE is less positive than ΔCRE^{af}. This difference is dominated by stronger clear-sky outgoing longwave radiation anomalies, caused by weaker longwave absorption and re-emission by some aerosols at lower temperatures. In general, ΔCRE is a more reasonable proxy for longwave ERF_{aci} than ΔCRE^{af}, because it includes the weak longwave aerosol contribution to the clear-sky outgoing longwave radiation anomaly, while the all-sky outgoing longwave radiation anomaly is nearly identical under aerosol-free and aerosol-inclusive conditions. This is broadly consistent with previous studies, including Zelinka et al. (2023), which use longwave ΔCRE as a practical proxy for longwave ERF_{aci}.

However, even in the longwave, cloud masking of non-cloud adjustments can still matter. In fixed-SST experiments, mild land cooling induced by aerosol forcing produces a positive surface Planck response, and this response is weaker in all-sky than in clear-sky conditions, yielding a positive cloud-masking effect that makes longwave ERF_{aci} less negative than would be inferred from ΔCRE alone. Lapse-rate adjustments associated with aerosol vertical structure may also contribute, especially in the presence of absorbing aerosol. In particular, relatively enhanced warming aloft can produce a more negative lapse-rate radiative response under all-sky than under clear-sky conditions, thereby yielding an additional positive cloud-masking effect, as in GFDL-AM4-MG2. By contrast, cloud masking of direct longwave aerosol effects is expected to be comparatively small, reflecting the generally weaker direct radiative influence of tropospheric aerosols in the longwave than in the shortwave.

One remaining feature is that, in the longwave, the aerosol-free cloud radiative kernel estimates are generally more extreme than the online double-call estimates: more negative in most cases where ERF_{aci} is negative, and more positive where ERF_{aci} is positive. A similar behavior is evident in Smith et al. (2020, their Fig. 11), with only one model exception. The more negative longwave estimates seen in most cases are not readily reconciled with the simple expectation based on positive cloud-masking contributions, although they do offset the opposite-signed cloud-masking contribution seen in the shortwave

https://doi.org/10.5194/egusphere-2026-6647
Preprint. Discussion started: 4 November 2026
© Author(s) 2026. CC BY 4.0 License.

cloud radiative kernel estimate. For present purposes, this behavior is best regarded as an unresolved feature rather than a settled physical interpretation.

The differences across methods are also evident in the spatial structure of the diagnosed forcing. Figures A2 and A3 show the zonal-mean distributions of shortwave and longwave ERF_{aci}, respectively, for each method and base-state climate. In the shortwave, the broad latitudinal patterns are generally similar across methods, as indicated by the high pattern correlations in Fig. A2, except for ΔCRE, whose correlations with the other methods are consistently lower, highlighting the importance of cloud masking of direct aerosol effects. Nevertheless, systematic differences remain in amplitude and in some regional features, such as the peak magnitude and the extent of subtropical weakening with warming. Thus, the main disagreement among methods arises less from a complete reorganization of the forcing pattern than from differences in the magnitude and regional expression of the diagnosed response. In the longwave, the patterns in Fig. A3 are likewise broadly similar across methods, with generally high correlations throughout. However, differences in peak amplitude and spatial structure, especially in GFDL-AM4-MG2 and in the colder base-states, appear to depend more on whether the cloud-masking effects of non-cloud adjustments are accounted for than on how aerosol vertical structure is treated.

Because total ERF_{aci} includes both shortwave and longwave contributions, the total panels inherit the shortwave-driven methodological bias, and aerosol-free methods therefore also tend to produce a stronger negative total ERF_{aci}. At the same time, the contrast between GFDL-AM4.0 and GFDL-AM4-MG2 shows that the diagnosed state-dependence of ERF_{aci} reflects both methodological bias and genuine physical differences in cloud response, considering the longwave contribution differs more substantially between the models. Overall, Fig. 2 shows that diagnostics based on aerosol-free conditions tend to overestimate ERF_{aci}, especially its shortwave component, and that the magnitude of this overestimate is itself climate-state dependent.

3.3 IRF_{ari} and ambiguity in partitioning

The decomposition issue is not confined to ERF_{aci}. Because aerosol forcing is partitioned into direct and cloud-mediated components, a bias in one term necessarily affects the other if the total forcing is to remain internally consistent. This is especially important for simpler diagnostics based on ΔCRE and clear-sky flux changes, in which ΔCRE is used as a proxy for ERF_{aci} and the corresponding clear-sky flux change is used as a proxy for IRF_{ari}. In this sense, the original motivation for the online double-call framework was to provide a more direct estimate of aerosol–radiation interactions and thereby reduce the ambiguity inherent in simpler diagnostics based on ΔCRE and clear-sky flux changes (Ghan, 2013). However, when aerosol-over-cloud attenuation biases the diagnosed cloud-mediated forcing, the inferred IRF_{ari} is also affected.

Figure 3 shows that the diagnosed IRF_{ari} depends on both decomposition method and base-state climate. Across both models, the shortwave component dominates the total IRF_{ari}, while the longwave contribution is much smaller, as expected for direct aerosol forcing. In the aerosol-inclusive methods, the shortwave IRF_{ari} generally weakens in magnitude as the base-state warms. A plausible interpretation is that warmer climates, with thicker and brighter clouds in aerosol-laden regions, reduce

https://doi.org/10.5194/egusphere-2026-6647
Preprint. Discussion started: 4 November 2026
© Author(s) 2026. CC BY 4.0 License.

the fraction of aerosol that interacts directly with radiation under all-sky conditions, thereby weakening the shortwave direct effect. In general, the APRP+kernels and radiative kernel estimates agree well, although modest differences remain in GFDL-AM4.0, with peak discrepancies of about 0.1 W m^{-2}. We return to the possible origin of this difference later in the section.

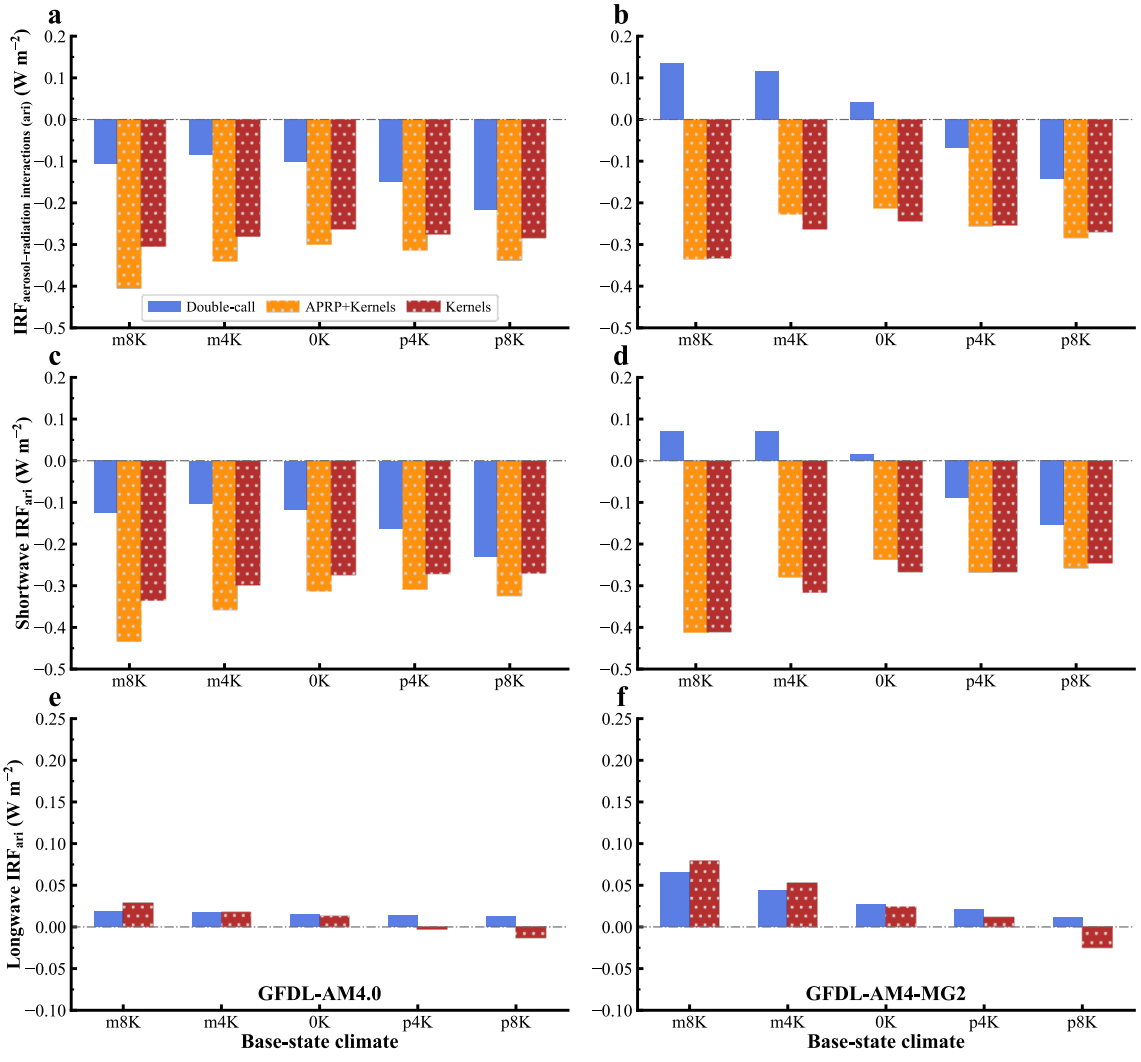


Figure 3: Total, shortwave, and longwave IRF_{ari} diagnosed using different decomposition methods across the five base-state climates. Rows from top to bottom show total, shortwave, and longwave results, respectively. The left column shows GFDL-AM4.0 and the right column shows GFDL-AM4-MG2. For each climate state, bars without overlaid dots indicate estimates from an aerosol-free decomposition method, whereas bars with overlaid dots indicate estimates from aerosol-inclusive methods. The vertical axis range in the bottom row is half that used in the top and middle rows.

By contrast, the aerosol-free online double-call method shows the opposite tendency in both models, with IRF_{ari} becoming more negative as the base-state warms. In GFDL-AM4-MG2, it even produces positive IRF_{ari} estimates in the colder base-states, including in the shortwave component. Positive shortwave IRF_{ari} is not necessarily physically implausible, particularly

https://doi.org/10.5194/egusphere-2026-6647
Preprint. Discussion started: 4 November 2026
© Author(s) 2026. CC BY 4.0 License.

when aerosol is located above or within clouds, where aerosol–cloud radiative interactions can modify the amount of shortwave radiation reflected to space and, under some conditions, produce a positive radiative effect. However, in this case, the positive IRF_{ari} estimates arise from an aerosol-free partition that is also affected by the aerosol-over-cloud bias discussed above, making their interpretation as a direct aerosol radiative effect particularly uncertain. More broadly, the differences among methods indicate that diagnosed IRF_{ari} is not independent of how ERF_{aci} is estimated. In colder base-states, where aerosol-over-cloud bias is strongest, aerosol-free methods that overestimate shortwave ERF_{aci} correspondingly diagnose a weaker, and sometimes even positive, shortwave IRF_{ari}. This follows directly from the partitioning in Eq. (9), using the notation of Ghan (2013): because the total ERF is decomposed into terms associated with IRF_{ari}, ERF_{aci}, and surface albedo changes, an overestimate of ERF_{aci}, represented by the second term, $\Delta(F^{af}–F^{clr,af})$, leaves a smaller residual for the first term, $\Delta(F−F^{af})$, and therefore leads to an underestimate of IRF_{ari}. The resulting bias is therefore opposite in sign to that found in ERF_{aci}. In warmer states, as aerosol-free and aerosol-inclusive estimates of ERF_{aci} move closer together, the corresponding IRF_{ari} estimates also become more similar.

The zonal-mean distributions further clarify how these method differences are expressed spatially. In the shortwave IRF_{ari} (Fig. A4), the broad latitudinal structures are less similar across methods than for ERF_{aci}. In particular, the aerosol-free online double-call estimate differs more strongly in amplitude and shows an opposite tendency with warming relative to the aerosol-inclusive APRP+kernels and radiative kernel estimates, consistent with the larger all-sky partitioning ambiguity under conditions where aerosol-over-cloud bias is strongest. Thus, the disagreement in Fig. 3 reflects not only differences in global-mean magnitude, but also systematic differences in the regional distribution of the inferred shortwave direct effect.

The longwave component changes much less across base-states, becoming only slightly less positive as the climate warms and thus providing a modest offset to the shortwave changes. Differences among methods are also small in magnitude, likely in part because of the comparatively weak longwave forcing. Although the zonal-mean distributions exhibit broadly consistent state-dependent behavior across methods and models, the spatial correlations between methods decrease as the base-state climate warms, resulting in relatively low mean correlations and large standard deviations across the five base states (Fig. A5). Nevertheless, the longwave contribution remains comparatively minor, reinforcing the conclusion that the main ambiguity in IRF_{ari} arises from the shortwave partition.

Figure 3 therefore highlights a broader ambiguity in forcing partitioning: methods that rely on aerosol-free radiative sensitivities, including the double-call method considered here, or otherwise neglect the effect of aerosol vertical structure on cloud radiative sensitivity, do not simply bias ERF_{aci} alone; they also alter the inferred balance between direct and cloud-mediated forcing more generally. Apparent trends in IRF_{ari} across climate states may therefore reflect not only genuine physical changes in aerosol–radiation interactions, but also methodological differences in how the total forcing is partitioned. In this sense, part of the diagnosed state-dependence of aerosol forcing components is a property of the decomposition framework itself.

https://doi.org/10.5194/egusphere-2026-6647
Preprint. Discussion started: 4 November 2026
© Author(s) 2026. CC BY 4.0 License.

The role of cloud masking in this ambiguity becomes clearer when the corresponding clear-sky IRF_{ari} estimates are compared across methods. Figure 4 shows the diagnosed clear-sky IRF_{ari} across methods and base-state climates. Compared with the all-sky results in Fig. 3, the clear-sky estimates show much closer agreement among methods, especially in the shortwave component. This is expected, since under clear-sky conditions the ambiguity associated with cloud masking is largely removed and the direct aerosol forcing can be diagnosed more directly.

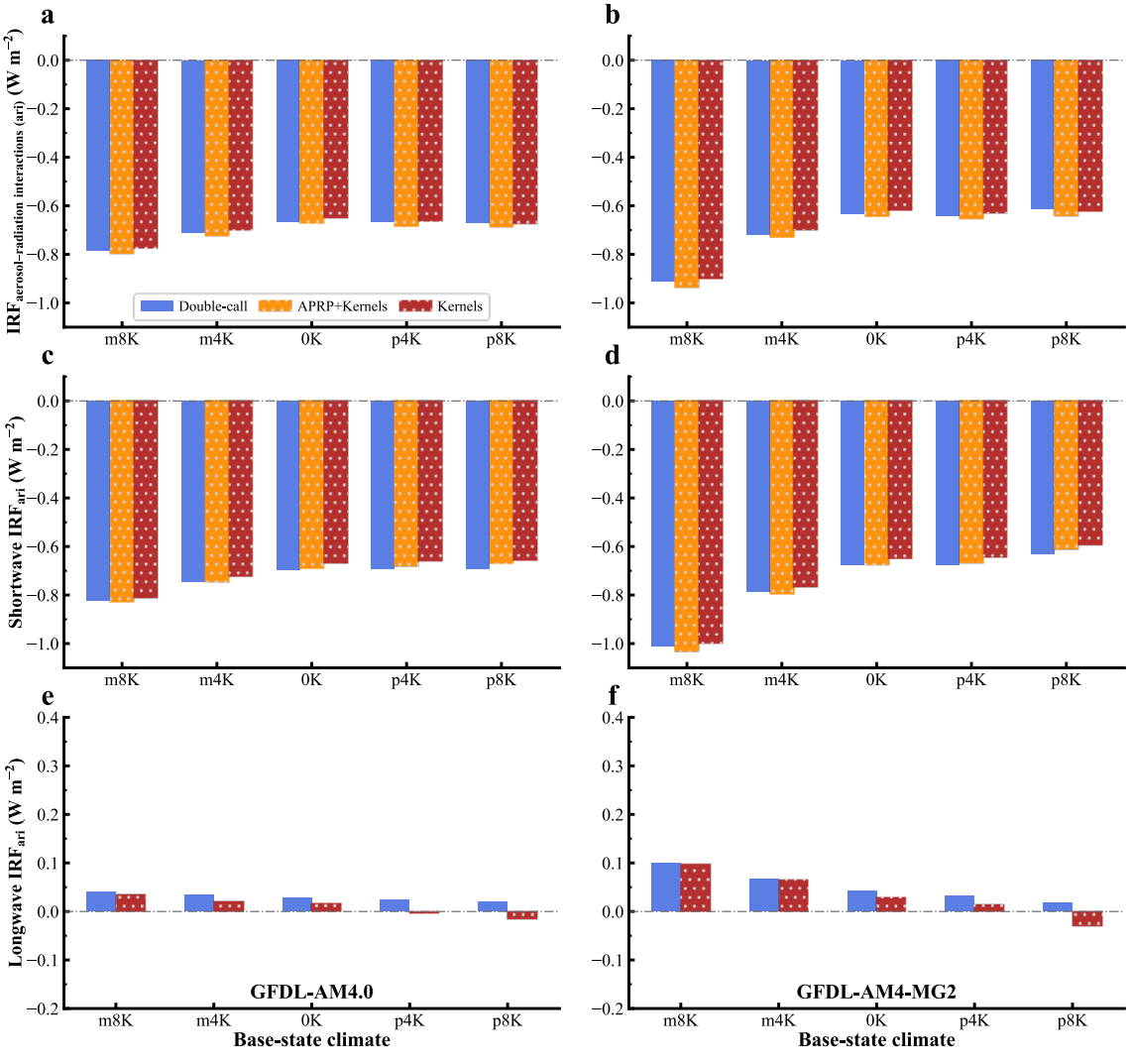


Figure 4: Clear-sky total, shortwave, and longwave IRF_{ari} diagnosed using different decomposition methods across the five base-state climates. Rows from top to bottom show total, shortwave, and longwave results, respectively. The left column shows GFDL-AM4.0 and the right column shows GFDL-AM4-MG2. For each climate state, bars without overlaid dots indicate estimates from an aerosol-free decomposition method, whereas bars with overlaid dots indicate estimates from aerosol-inclusive methods. The vertical axis range in the bottom row is half that used in the top and middle rows.

https://doi.org/10.5194/egusphere-2026-6647
Preprint. Discussion started: 4 November 2026
© Author(s) 2026. CC BY 4.0 License.

Across both models, the shortwave component remains the dominant contribution to clear-sky IRF_{ari}, while the longwave contribution is comparatively small. The clear-sky shortwave IRF_{ari} generally weakens in magnitude as the base-state warms, likely reflecting stronger wet deposition in warmer climates and therefore a shorter lifetime of anthropogenic aerosol (Fig. A1), which also contributes to the broader weakening of direct aerosol forcing with warming. In this context, the clear-sky online double-call estimate can be regarded as a practical benchmark, since there are few obvious sources of bias in its diagnosis under clear-sky conditions. The relatively small spread across methods in Fig. 4 therefore suggests that much of the stronger method dependence seen in all-sky IRF_{ari} arises from how cloud effects are partitioned, rather than from disagreement in the clear-sky aerosol–radiation interaction itself.

Consistent with this interpretation, APRP+kernels and radiative kernel estimates differ little from the online double-call results in the shortwave, reflecting both the relatively weak state-dependence of shortwave radiative sensitivities to unit perturbations in surface albedo and water vapor (Jonko et al., 2012) and the small changes in those fields across the experiments. Notably, the near-identical APRP+kernels and radiative kernel estimates under clear-sky conditions contrast with the small differences between them under all-sky conditions. This likely reflects the use of a constant cloud-masking factor in the all-sky radiative kernel estimates, which may vary somewhat across models and therefore not be represented exactly, even though it generally captures the correct magnitude. Some discrepancy does emerge in the longwave, particularly as the base-state warms. A plausible explanation is that, under warming, the longwave radiative sensitivity to unit surface temperature perturbations becomes less negative because the atmosphere is more opaque owing to increased water vapor (Jonko et al., 2012). As a result, the surface Planck response to land cooling may be overestimated when diagnosed using radiative kernels derived from a relatively cooler base-state, yielding a residual longwave clear-sky IRF_{ari} that is biased low. However, because land cooling in fixed-SST configurations is weak and the longwave IRF_{ari} itself is small, this effect does not undermine the overall utility of the APRP+kernels and radiative kernel estimates. Taken together, Figs. 3 and 4 indicate that the pronounced method dependence in IRF_{ari}, including anomalous values in some aerosol-free estimates, arises primarily from all-sky partitioning and cloud masking rather than from the underlying clear-sky direct aerosol effect.

4 Recommendations for interpretation and application

The results above have several practical implications for the diagnosis and interpretation of aerosol forcing. The central issue is not that any single decomposition framework is universally invalid, but that commonly used methods differ in two important respects: how they treat aerosol vertical structure, which affects the radiative sensitivity of cloud perturbations, and whether they account for the cloud-masking effects of non-cloud adjustments and direct aerosol forcing. These differences become especially important when decomposed forcing is compared across climate states, which provide a useful test bed for revealing methodological sensitivities that may remain hidden in a single base-state. Assessment across a broad range of background climates therefore gives a more meaningful evaluation of the general accuracy and robustness of a

https://doi.org/10.5194/egusphere-2026-6647
Preprint. Discussion started: 4 November 2026
© Author(s) 2026. CC BY 4.0 License.

520 decomposition method than does assessment in only one climate state. The main strengths, limitations, and guidance for applying these methods across climate states are summarized in Table 2.

Table 2. Strengths, limitations, and guidance for the application of aerosol-forcing decomposition methods.

Method	Main strengths and best use	Main limitations	Guidance for climate-state comparisons
ΔCRE / clear-sky flux change	**Simple and widely available** from standard model output; useful as first-order proxies for ERF_{aci} and IRF_{ari}	**Not a unique physical partition**. ΔCRE contains cloud masking of non-cloud adjustments and direct aerosol effects, while the clear-sky flux change does not capture the full all-sky IRF_{ari}	**Use primarily as first-order proxies**, particularly in SW. Apparent state-dependence may reflect changes in cloud masking and aerosol–cloud geometry as well as physical changes in ERF_{aci} or IRF_{ari}
Radiative kernels	**Quantitative SW and LW decomposition** of ERF_{aci}, IRF_{ari}, and non-cloud adjustments; corrects ERF_{aci} for cloud masking of non-cloud adjustments and direct aerosol effects using standard model output.	**Sensitive to kernel assumptions**. Depends on kernel linearity and background-state dependence; all-sky IRF_{ari} also requires an assumed cloud-masking factor.	**Well suited for quantitative cross-state comparisons**, but kernel sensitivity and the assumed IRF_{ari} cloud-masking factor should be assessed when background climates differ substantially
APRP	**Physically interpretable SW decomposition** into cloud, non-cloud atmospheric, and surface-albedo contributions; useful for quantitative SW ERF_{aci} and IRF_{ari} diagnosis.	**Limited to SW** and approximate, based on a one-layer radiative-transfer framework	**Well suited for SW cross-state comparisons** because aerosol radiative effects are retained in the underlying fluxes
Online double-call	**Direct diagnosis using the model's native radiation scheme**; particularly useful for IRF_{ari}, with clear-sky IRF_{ari} providing a useful benchmark	**Aerosol-free ERFaci does not represent aerosol-over-cloud attenuation**. ΔCRE^{af} can also retain cloud masking of non-cloud adjustments; additional online radiation calls are required	**Use caution for all-sky forcing partitions**. State-dependent changes in aerosol–cloud vertical overlap can produce state-dependent biases in SW ERF_{aci} and, through partition consistency, corresponding biases in IRF_{ari}
Cloud radiative kernels	**Detailed mechanistic diagnosis of cloud radiative changes** by cloud amount, optical depth/scattering, altitude, and cloud regime;	**Aerosol-over-cloud attenuation is generally not represented**, because cloud radiative sensitivities are most commonly derived without aerosol	**Useful for structural and mechanistic comparisons across climate states**, but quantitative SW ERF_{aci} trends should be interpreted cautiously when aerosol-over-

https://doi.org/10.5194/egusphere-2026-6647
Preprint. Discussion started: 4 November 2026
© Author(s) 2026. CC BY 4.0 License.

particularly useful for interpreting the structure of ERF_{aci}	radiative effects; cloud-simulator output and precomputed kernels are also required	cloud occurrence changes with climate

Aerosol vertical structure should be accounted for whenever possible. At a minimum, studies should assess whether aerosol perturbations reside primarily above, within, or below cloud layers, since this geometry directly affects the shortwave radiative sensitivity of cloud changes. When aerosols are located above clouds, aerosol-free diagnostics tend to overestimate shortwave ERF_{aci} because they neglect attenuation of incoming solar radiation before it reaches cloud top. For this reason, aerosol-free radiative sensitivities should not be interpreted as exact shortwave cloud sensitivities in the presence of overlying aerosol. This applies both to aerosol-free cloud radiative kernel methods and to aerosol-free double-call frameworks. In such cases, the diagnosed ERF_{aci} is biased high, and the inferred IRF_{ari} in the double-call framework is correspondingly biased low through partition consistency. More generally, methods that neglect aerosol-over-cloud attenuation can misallocate forcing between direct and cloud-mediated components.

ERF partitions should therefore be interpreted cautiously when comparing across climate states or across models with different aerosol and cloud climatologies. Apparent changes in the relative importance of aerosol–radiation and aerosol–cloud interaction forcing may reflect the diagnostic framework as much as the underlying physics. In particular, part of the diagnosed state-dependence of ERF_{aci} and IRF_{ari} may arise from methodological bias rather than from a true physical change in aerosol forcing. In the present case, this is illustrated by the shortwave aerosol-over-cloud effect, which introduces a diagnostic bias that makes ERF_{aci} too strong and the corresponding IRF_{ari} too weak, with the bias being more pronounced in colder climates and weakening as the climate warms. Such changes should therefore not be interpreted as purely physical without first accounting for the state-dependence of the decomposition method itself.

Total ERF should always be reported alongside any partition into components. Although fixed-SST simulations still permit some land cooling, which can introduce a small bias into the diagnosed ERF, total ERF remains less sensitive than the component terms to the methodological ambiguities discussed here and therefore provides a more robust basis for model comparison and physical interpretation. Component partitions remain useful, but they should be treated as method dependent rather than uniquely physical when aerosol-over-cloud effects and cloud masking are important.

Based on these considerations, aerosol-inclusive decomposition methods are preferable when the goal is to estimate ERF_{aci} across different climate states. Among the approaches examined here, the APRP+kernels and radiative kernel methods provide the most physically consistent framework for shortwave decomposition because they more explicitly account for aerosol-over-cloud attenuation and avoid the strongest biases associated with aerosol-free diagnostics. Although they do not eliminate all ambiguity, since cloud masking of non-cloud adjustments and direct aerosol effects still matters, they are less vulnerable than aerosol-free methods to the systematic bias introduced by aerosol-over-cloud attenuation. The radiative kernel method is also advantageous for the longwave component because it captures land-cooling-related adjustments and

https://doi.org/10.5194/egusphere-2026-6647
Preprint. Discussion started: 4 November 2026
© Author(s) 2026. CC BY 4.0 License.

their associated cloud-masking effects. Since both methods can be applied using standard model output, they are especially well suited for model intercomparison. The state-dependence of radiative kernels themselves remains a potential concern, but in fixed-SST simulations the associated land temperature changes are generally small, so this source of bias is expected to be secondary here. By contrast, ΔCRE should be regarded primarily as a proxy rather than as a direct estimate of ERF_{aci}, and aerosol-free cloud radiative kernel and double-call estimates should be interpreted with particular caution when aerosols are likely to reside above clouds.

Overall, aerosol forcing decomposition remains highly valuable, but its interpretation requires explicit attention to aerosol vertical structure, cloud masking, and base-state dependence. When these effects cannot be fully represented within the diagnostic framework, the safest approach is to emphasize total ERF and to treat the partition into components as conditional on the method used rather than as a uniquely defined physical quantity.

https://doi.org/10.5194/egusphere-2026-6647
Preprint. Discussion started: 4 November 2026
© Author(s) 2026. CC BY 4.0 License.

5 Appendices

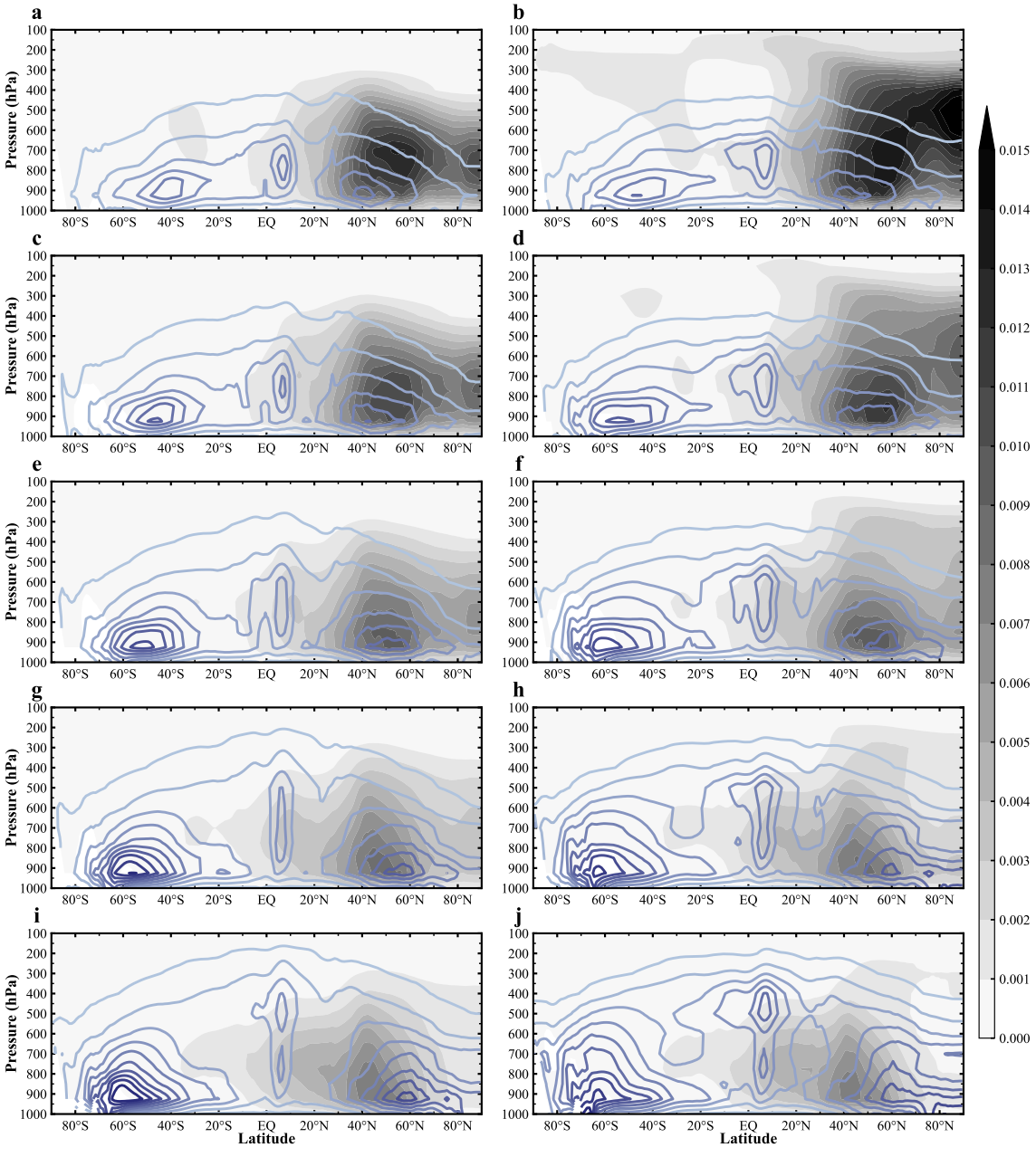
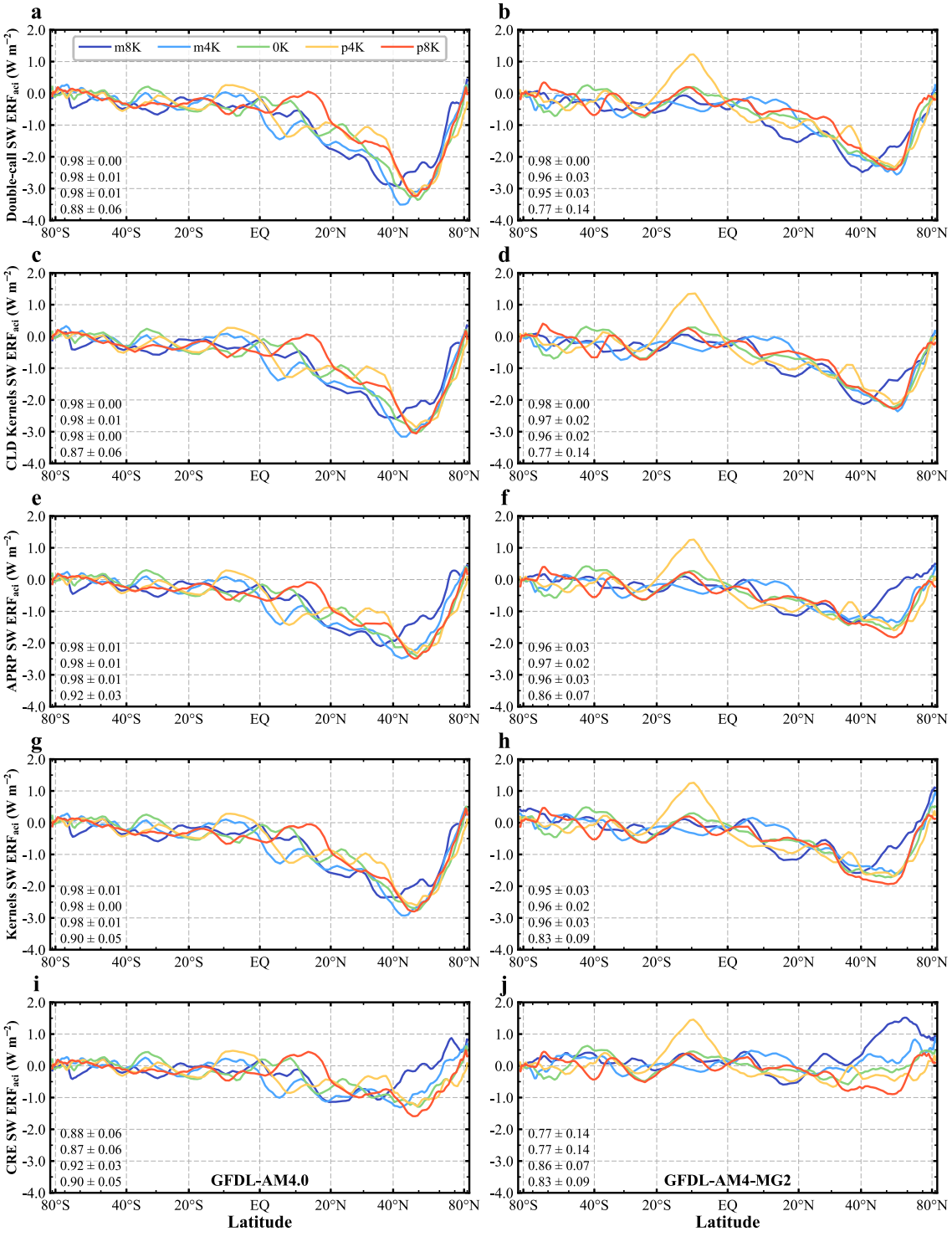


Figure A1: Vertical distribution of zonal-mean aerosol optical depth (AOD) anomalies and climatological cloud liquid water content across the five base-state climates. From top to bottom, rows correspond to m8K, m4K, 0K, p4K, and p8K. The left column shows GFDL-AM4.0 and the right column shows GFDL-AM4-MG2. Shading denotes the AOD anomaly between the present-day and preindustrial aerosol simulations, and contours show the climatological present-day cloud liquid water content. Contour levels start at 1×10^{-6} kg kg^{-1}, followed by evenly spaced intervals of 5×10^{-6} kg kg^{-1} from 5×10^{-6} to 5×10^{-5} kg kg^{-1}.

https://doi.org/10.5194/egusphere-2026-6647
Preprint. Discussion started: 4 November 2026
© Author(s) 2026. CC BY 4.0 License.



570

https://doi.org/10.5194/egusphere-2026-6647
Preprint. Discussion started: 4 November 2026
© Author(s) 2026. CC BY 4.0 License.



Figure A2: Zonal-mean distributions of shortwave ERF_{aci} diagnosed using different decomposition methods across the five base-state climates. Rows from top to bottom show results from the aerosol-free online double-call and cloud radiative kernel methods, followed by the aerosol-inclusive APRP, radiative kernel, and CRE proxy methods. The left column shows GFDL-AM4.0 and the right column shows GFDL-AM4-MG2. Colored lines denote the five base-state climates (m8K, m4K, 0K, p4K, and p8K). The numbers shown in the lower left of each panel give the mean ± one standard deviation of the spatial pattern correlation coefficients between the method shown in that panel and each of the other four methods listed from top to bottom. For each method pair, the spatial pattern correlation is calculated separately for each of the five base-state climates, comparing the same base state between the two methods, and the mean and standard deviation are then calculated across the five resulting correlation coefficients.

https://doi.org/10.5194/egusphere-2026-6647
Preprint. Discussion started: 4 November 2026
© Author(s) 2026. CC BY 4.0 License.

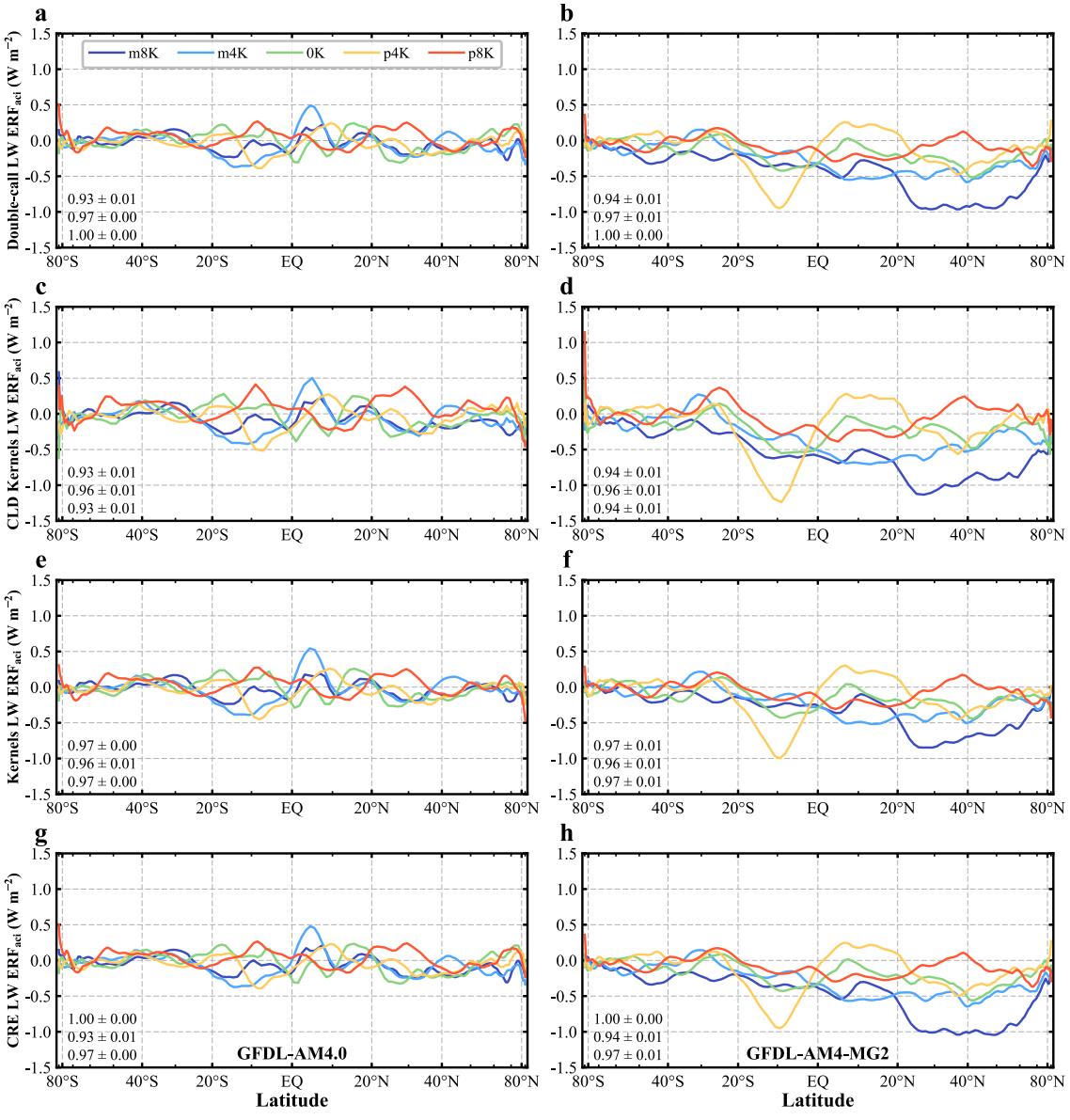


Figure A3: Zonal-mean distributions of longwave ERF$_{aci}$ diagnosed using different decomposition methods across the five base-state climates. Rows from top to bottom show results from the aerosol-free online double-call and cloud radiative kernel methods, followed by the aerosol-inclusive radiative kernel and CRE proxy methods. The left column shows GFDL-AM4.0 and the right column shows GFDL-AM4-MG2. Colored lines denote the five base-state climates (m8K, m4K, 0K, p4K, and p8K). The numbers shown in the lower left of each panel give the mean ± one standard deviation of the spatial pattern correlation coefficients between the method shown in that panel and each of the other three methods listed from top to bottom. For each method pair, the spatial pattern correlation is calculated separately for each of the five base-state climates, comparing the same base state between the two methods, and the mean and standard deviation are then calculated across the five resulting correlation coefficients.

https://doi.org/10.5194/egusphere-2026-6647
Preprint. Discussion started: 4 November 2026
© Author(s) 2026. CC BY 4.0 License.

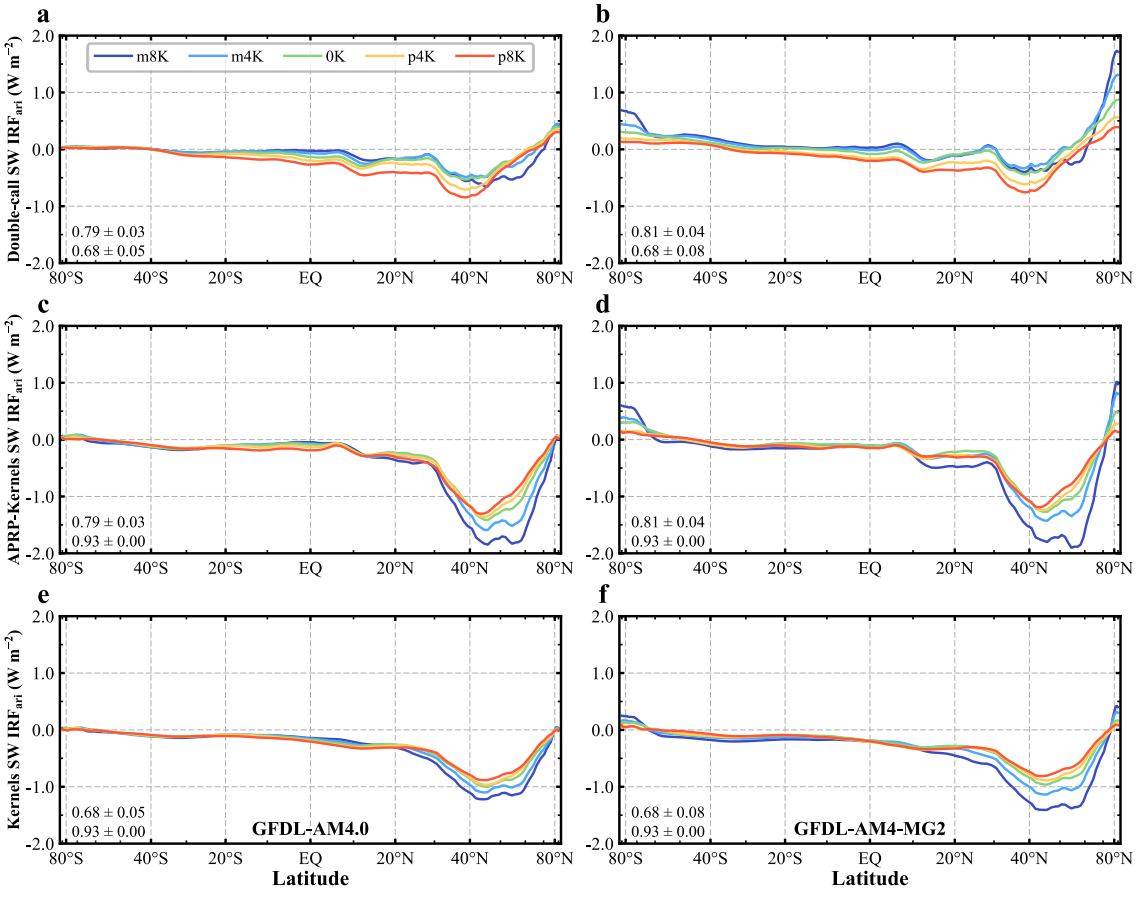


Figure A4: Zonal-mean distributions of shortwave IRF$_{ari}$ diagnosed using different decomposition methods across the five base-state climates. Rows from top to bottom show results from the aerosol-free online double-call method, followed by the aerosol-inclusive APRP+kernels and radiative kernel methods. The left column shows GFDL-AM4.0 and the right column shows GFDL-AM4-MG2. Colored lines denote the five base-state climates (m8K, m4K, 0K, p4K, and p8K). The numbers shown in the lower left of each panel give the mean ± one standard deviation of the spatial pattern correlation coefficients between the method shown in that panel and each of the other two methods listed from top to bottom. For each method pair, the spatial pattern correlation is calculated separately for each of the five base-state climates, comparing the same base state between the two methods, and the mean and standard deviation are then calculated across the five resulting correlation coefficients.

https://doi.org/10.5194/egusphere-2026-6647
Preprint. Discussion started: 4 November 2026
© Author(s) 2026. CC BY 4.0 License.

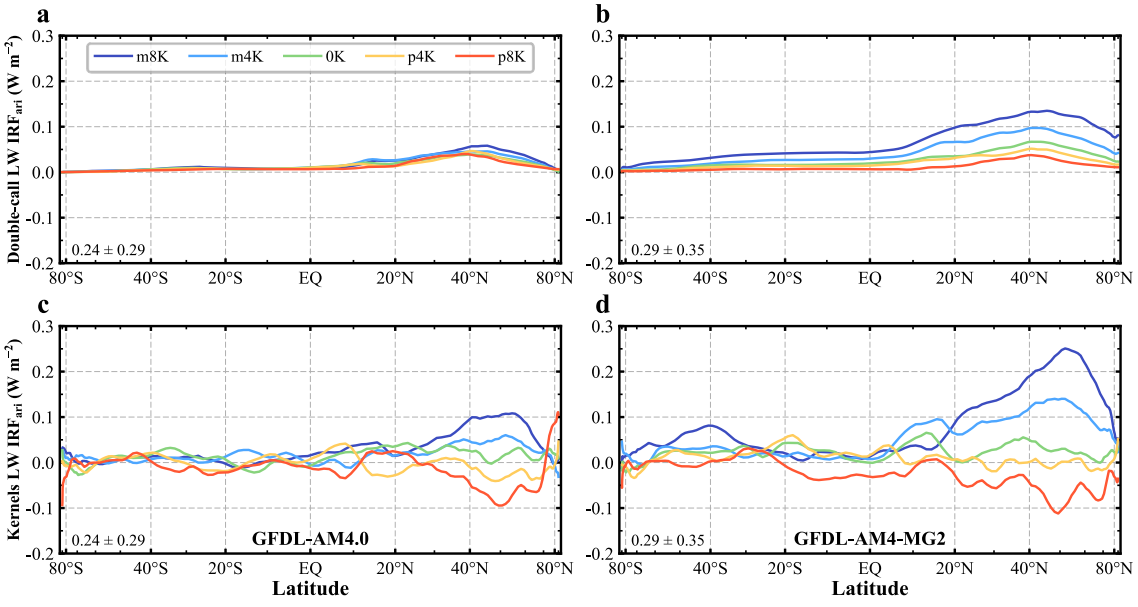


Figure A5: Zonal-mean distributions of longwave IRF$_{ari}$ diagnosed using different decomposition methods across the five base-state climates. Rows from top to bottom show results from the aerosol-free online double-call method and the aerosol-inclusive radiative kernel method. The left column shows GFDL-AM4.0 and the right column shows GFDL-AM4-MG2. Colored lines denote the five base-state climates (m8K, m4K, 0K, p4K, and p8K). The numbers shown in the lower left of each panel give the mean ± one standard deviation of the spatial pattern correlation coefficients between the method shown in that panel and the other method listed. For each method pair, the spatial pattern correlation is calculated separately for each of the five base-state climates, comparing the same base state between the two methods, and the mean and standard deviation are then calculated across the five resulting correlation coefficients.

https://doi.org/10.5194/egusphere-2026-6647
Preprint. Discussion started: 4 November 2026
© Author(s) 2026. CC BY 4.0 License.

Code and data availability

The processed data and Python scripts used to produce the figures in this study are publicly available on Zenodo (He, 2026; https://doi.org/10.5281/zenodo.23696850).

Author contributions

HH performed all simulations and analyses and prepared the initial draft of the manuscript. All authors contributed to reviewing and revising the manuscript and read and approved the final version.

Competing interests

Authors have no competing interests.

Acknowledgements

We thank Dr. David Paynter for helpful comments. We also thank Dr. Huan Guo for providing the necessary files and clarifying the namelist modifications required to use GFDL-AM4-MG2.

Financial support

H.H., B.J.S., and G.A.V. were supported by Award MPS-SRM-00006584 from the Simons Foundation. R.J.K. acknowledges support from the National Oceanic and Atmospheric Administration, U.S. Department of Commerce. The statements, findings, conclusions, and recommendations are those of the author(s) and do not necessarily reflect the views of the National Oceanic and Atmospheric Administration, or the U.S. Department of Commerce. J.Z. acknowledges the support by the U.S. Department of Commerce, Earth's Radiation Budget grant, NOAA CPO Climate & CI #03-01-07-001 and the NOAA Cooperative Agreement with CIRES, NA22OAR4320151. C.P. was supported by the NASA grant 80NSSC23K0115.

References

Ackerman, A. S., Toon, O. B., Stevens, D. E., Heymsfield, A. J., Ramanathan, V., and Welton, E. J.: Reduction of Tropical Cloudiness by Soot, Science, 288, 1042–1047, https://doi.org/10.1126/science.288.5468.1042, 2000.

Albrecht, B. A.: Aerosols, Cloud Microphysics, and Fractional Cloudiness, Science, 245, 1227–1230, https://doi.org/10.1126/science.245.4923.1227, 1989.

https://doi.org/10.5194/egusphere-2026-6647
Preprint. Discussion started: 4 November 2026
© Author(s) 2026. CC BY 4.0 License.

Bellouin, N., Quaas, J., Gryspeerdt, E., Kinne, S., Stier, P., Watson-Parris, D., Boucher, O., Carslaw, K. S., Christensen, M., Daniau, A. -L., Dufresne, J. -L., Feingold, G., Fiedler, S., Forster, P., Gettelman, A., Haywood, J. M., Lohmann, U., Malavelle, F., Mauritsen, T., McCoy, D. T., Myhre, G., Mülmenstädt, J., Neubauer, D., Possner, A., Rugenstein, M., Sato, Y., Schulz, M., Schwartz, S. E., Sourdeval, O., Storelvmo, T., Toll, V., Winker, D., and Stevens, B.: Bounding Global Aerosol Radiative Forcing of Climate Change, Rev. Geophys., 58, e2019RG000660, https://doi.org/10.1029/2019rg000660, 2020.

Bender, F. A.-M., Frey, L., McCoy, D. T., Grosvenor, D. P., and Mohrmann, J. K.: Assessment of aerosol–cloud–radiation correlations in satellite observations, climate models and reanalysis, Clim. Dyn., 52, 4371–4392, https://doi.org/10.1007/s00382-018-4384-z, 2019.

Boucher, O., Randall, D., Artaxo, P., Bretherton, C., Feingold, G., Forster, P., Kerminen, V.-M., Kondo, Y., Liao, H., Lohmann, U., Rasch, P., Satheesh, S. K., Sherwood, S., Stevens, B., and Zhang, X. Y.: Clouds and Aerosols, in: Climate Change 2013: The Physical Science Basis. Contribution of Working Group I to the Fifth Assessment Report of the Intergovernmental Panel on Climate Change, edited by: Stocker, T. F., Qin, D., Plattner, G.-K., Tignor, M., Allen, S. K., Boschung, J., Nauels, A., Xia, Y., Bex, V., and Midgley, P. M., Cambridge University Press, Cambridge, United Kingdom and New York, NY, USA, 571–659, https://doi.org/10.1017/cbo9781107415324.016, 2013.

Bretherton, C. S., Blossey, P. N., and Uchida, J.: Cloud droplet sedimentation, entrainment efficiency, and subtropical stratocumulus albedo, Geophys. Res. Lett., 34, L03813, https://doi.org/10.1029/2006GL027648, 2007.

Chen, W. -T., Lee, Y. H., Adams, P. J., Nenes, A., and Seinfeld, J. H.: Will black carbon mitigation dampen aerosol indirect forcing?, Geophys. Res. Lett., 37, https://doi.org/10.1029/2010gl042886, 2010.

Chen, Y.-C., Christensen, M. W., Stephens, G. L., and Seinfeld, J. H.: Satellite-based estimate of global aerosol–cloud radiative forcing by marine warm clouds, Nat. Geosci., 7, 643–646, https://doi.org/10.1038/ngeo2214, 2014.

Christensen, M. W., Neubauer, D., Poulsen, C. A., Thomas, G. E., McGarragh, G. R., Povey, A. C., Proud, S. R., and Grainger, R. G.: Unveiling aerosol–cloud interactions – Part 1: Cloud contamination in satellite products enhances the aerosol indirect forcing estimate, Atmos. Chem. Phys., 17, 13151–13164, https://doi.org/10.5194/acp-17-13151-2017, 2017.

Fan, S., Ginoux, P., Seman, C. J., Silvers, L. G., and Zhao, M.: Towards Improved Cloud-Phase Simulation with a Mineral Dust and Temperature-Dependent Parameterization for Ice Nucleation in Mixed-Phase Clouds Towards Improved Cloud-Phase Simulation with a Mineral Dust and Temperature-Dependent Parameterization for Ice Nucleation in Mixed-Phase Clouds, J. Atmos. Sci., 76, 3655–3667, https://doi.org/10.1175/jas-d-18-0287.1, 2019.

Forster, P., Ramaswamy, V., Artaxo, P., Berntsen, T., Betts, R., Fahey, D. W., Haywood, J., Lean, J., Lowe, D. C., Myhre, G., Nganga, J., Prinn, R., Raga, G., Schulz, M., and Dorland, R. V.: Changes in Atmospheric Constituents and in Radiative Forcing, in: Climate Change 2007: The Physical Science Basis. Contribution of Working Group I to the Fourth Assessment

https://doi.org/10.5194/egusphere-2026-6647
Preprint. Discussion started: 4 November 2026
© Author(s) 2026. CC BY 4.0 License.

Report of the Intergovernmental Panel on Climate Change, edited by: Solomon, S., Qin, D., Manning, M., Chen, Z., Marquis, M., Averyt, K. B., M.Tignor, and Miller, H. L., Cambridge University Press, Cambridge, United Kingdom and New York, NY, USA, 129–234, 2007.

Forster, P. M., Richardson, T., Maycock, A. C., Smith, C. J., Samset, B. H., Myhre, G., Andrews, T., Pincus, R., and Schulz, M.: Recommendations for diagnosing effective radiative forcing from climate models for CMIP6, J. Geophys. Res.: Atmos., 121, 12,460-12,475, https://doi.org/10.1002/2016jd025320, 2016.

Forster, P., Storelvmo, T., Armour, K., Collins, W., Dufresne, J.-L., Frame, D., Lunt, D. J., Mauritsen, T., Palmer, M. D., Watanabe, M., Wild, M., and Zhang, H.: The Earth's Energy Budget, Climate Feedbacks and Climate Sensitivity, in: Climate Change 2021: The Physical Science Basis. Contribution of Working Group I to the Sixth Assessment Report of the Intergovernmental Panel on Climate Change, edited by: Masson-Delmotte, V., Zhai, P., Pirani, A., Connors, S. L., Péan, C., Berger, S., Caud, N., Chen, Y., Goldfarb, L., Gomis, M. I., Huang, M., Leitzell, K., Lonnoy, E., Matthews, J. B. R., Maycock, T. K., Waterfield, T., Yelekçi, O., Yu, R., and Zhou, B., Cambridge University Press, Cambridge, United Kingdom and New York, NY, USA, 923–1054, https://doi.org/10.1017/9781009157896.009, 2021.

Gelaro, R., McCarty, W., Suárez, M. J., Todling, R., Molod, A., Takacs, L., Randles, C. A., Darmenov, A., Bosilovich, M. G., Reichle, R., Wargan, K., Coy, L., Cullather, R., Draper, C., Akella, S., Buchard, V., Conaty, A., Silva, A. M. da, Gu, W., Kim, G.-K., Koster, R., Lucchesi, R., Merkova, D., Nielsen, J. E., Partyka, G., Pawson, S., Putman, W., Rienecker, M., Schubert, S. D., Sienkiewicz, M., and Zhao, B.: The Modern-Era Retrospective Analysis for Research and Applications, Version 2 (MERRA-2), J. Clim., 30, 5419–5454, https://doi.org/10.1175/jcli-d-16-0758.1, 2017.

Gettelman, A., Liu, X., Barahona, D., Lohmann, U., and Chen, C.: Climate impacts of ice nucleation, J. Geophys. Res.: Atmos., 117, https://doi.org/10.1029/2012jd017950, 2012.

Gettelman, A. and Morrison, H.: Advanced Two-Moment Bulk Microphysics for Global Models. Part I: Off-Line Tests and Comparison with Other Schemes, J. Clim., 28, 1268–1287, https://doi.org/10.1175/jcli-d-14-00102.1, 2015.

Ghan, S. J.: Technical Note: Estimating aerosol effects on cloud radiative forcing, Atmos. Chem. Phys., 13, 9971–9974, https://doi.org/10.5194/acp-13-9971-2013, 2013.

Ghan, S., Wang, M., Zhang, S., Ferrachat, S., Gettelman, A., Griesfeller, J., Kipling, Z., Lohmann, U., Morrison, H., Neubauer, D., Partridge, D. G., Stier, P., Takemura, T., Wang, H., and Zhang, K.: Challenges in constraining anthropogenic aerosol effects on cloud radiative forcing using present-day spatiotemporal variability, Proc. Natl. Acad. Sci., 113, 5804–5811, https://doi.org/10.1073/pnas.1514036113, 2016.

Glassmeier, F., Hoffmann, F., Johnson, J. S., Yamaguchi, T., Carslaw, K. S., and Feingold, G.: Aerosol-cloud-climate cooling overestimated by ship-track data, Science, 371, 485–489, https://doi.org/10.1126/science.abd3980, 2021.

https://doi.org/10.5194/egusphere-2026-6647
Preprint. Discussion started: 4 November 2026
© Author(s) 2026. CC BY 4.0 License.

Gryspeerdt, E., Goren, T., Sourdeval, O., Quaas, J., Mülmenstädt, J., Dipu, S., Unglaub, C., Gettelman, A., and Christensen, M.: Constraining the aerosol influence on cloud liquid water path, Atmos. Chem. Phys., 19, 5331–5347, https://doi.org/10.5194/acp-19-5331-2019, 2019.

Gryspeerdt, E., Mülmenstädt, J., Gettelman, A., Malavelle, F. F., Morrison, H., Neubauer, D., Partridge, D. G., Stier, P., Takemura, T., Wang, H., Wang, M., and Zhang, K.: Surprising similarities in model and observational aerosol radiative forcing estimates, Atmos. Chem. Phys., 20, 613–623, https://doi.org/10.5194/acp-20-613-2020, 2020.

Gryspeerdt, E., Quaas, J., Ferrachat, S., Gettelman, A., Ghan, S., Lohmann, U., Morrison, H., Neubauer, D., Partridge, D. G., Stier, P., Takemura, T., Wang, H., Wang, M., and Zhang, K.: Constraining the instantaneous aerosol influence on cloud albedo, Proc. Natl. Acad. Sci., 114, 4899–4904, https://doi.org/10.1073/pnas.1617765114, 2017.

Guo, H., Ming, Y., Fan, S., Zhou, L., Harris, L., and Zhao, M.: Two-Moment Bulk Cloud Microphysics With Prognostic Precipitation in GFDL's Atmosphere Model AM4.0: Configuration and Performance, J. Adv. Model. Earth Syst., 13, https://doi.org/10.1029/2020ms002453, 2021.

Hansen, J., Sato, M., and Ruedy, R.: Radiative forcing and climate response, J. Geophys. Res.: Atmos., 102, 6831–6864, https://doi.org/10.1029/96jd03436, 1997.

Hansen, J., Sato, M., Ruedy, R., Nazarenko, L., Lacis, A., Schmidt, G. A., Russell, G., Aleinov, I., Bauer, M., Bauer, S., Bell, N., Cairns, B., Canuto, V., Chandler, M., Cheng, Y., Genio, A. D., Faluvegi, G., Fleming, E., Friend, A., Hall, T., Jackman, C., Kelley, M., Kiang, N., Koch, D., Lean, J., Lerner, J., Lo, K., Menon, S., Miller, R., Minnis, P., Novakov, T., Oinas, V., Perlwitz, Ja., Perlwitz, Ju., Rind, D., Romanou, A., Shindell, D., Stone, P., Sun, S., Tausnev, N., Thresher, D., Wielicki, B., Wong, T., Yao, M., and Zhang, S.: Efficacy of climate forcings, J. Geophys. Res.: Atmos., 110, https://doi.org/10.1029/2005jd005776, 2005.

Haywood, J. and Boucher, O.: Estimates of the direct and indirect radiative forcing due to tropospheric aerosols: A review, Rev. Geophys., 38, 513–543, https://doi.org/10.1029/1999rg000078, 2000.

Haywood, J. M., Donner, L. J., Jones, A., and Golaz, J.-C.: Global indirect radiative forcing caused by aerosols: IPCC (2007) and beyond, in: Clouds in the Perturbed Climate System: Their Relationship to Energy Balance, Atmospheric Dynamics, and Precipitation, edited by: Heintzenberg, J. and Charlson, R. J., MIT Press, Cambridge, 451–467, 2009.

He, H.: Data and scripts used to produce the figures for "Technical note: Aerosol forcing decomposition methods and recommendations", Zenodo [data set], https://doi.org/10.5281/zenodo.23696850, 2026.

He, H., Soden, B. J., Vecchi, G. A., Kramer, R. J., Zhang, J., and Park, C.: State dependence of aerosol forcing and its implications for climate response, 2026.

https://doi.org/10.5194/egusphere-2026-6647
Preprint. Discussion started: 4 November 2026
© Author(s) 2026. CC BY 4.0 License.

He, H., Soden, B., Zhang, B., Vecchi, G., and Yang, W.: State dependence of cloud feedback and its implications for climate sensitivity, PREPRINT (Version 1) available at Research Square, https://doi.org/10.21203/rs.3.rs-5220475/v1, 2024.

Hoose, C., Kristjánsson, J. E., Iversen, T., Kirkevåg, A., Seland, Ø., and Gettelman, A.: Constraining cloud droplet number concentration in GCMs suppresses the aerosol indirect effect, Geophys. Res. Lett., 36, https://doi.org/10.1029/2009gl038568, 2009.

Jonko, A. K., Shell, K. M., Sanderson, B. M., and Danabasoglu, G.: Climate Feedbacks in CCSM3 under Changing CO2 Forcing. Part I: Adapting the Linear Radiative Kernel Technique to Feedback Calculations for a Broad Range of Forcings, J. Clim., 25, 5260–5272, https://doi.org/10.1175/jcli-d-11-00524.1, 2012.

Kramer, R. J., He, H., Soden, B. J., Oreopoulos, L., Myhre, G., Forster, P. M., and Smith, C. J.: Observational Evidence of Increasing Global Radiative Forcing, Geophys. Res. Lett., 48, https://doi.org/10.1029/2020gl091585, 2021.

Lohmann, U., Rotstayn, L., Storelvmo, T., Jones, A., Menon, S., Quaas, J., Ekman, A. M. L., Koch, D., and Ruedy, R.: Total aerosol effect: radiative forcing or radiative flux perturbation?, Atmos. Chem. Phys., 10, 3235–3246, https://doi.org/10.5194/acp-10-3235-2010, 2010.

Myhre, G., Forster, P. M., Samset, B. H., Hodnebrog, Ø., Sillmann, J., Aalbergsjø, S. G., Andrews, T., Boucher, O., Faluvegi, G., Fläschner, D., Iversen, T., Kasoar, M., Kharin, V., Kirkevåg, A., Lamarque, J.-F., Olivié, D., Richardson, T. B., Shindell, D., Shine, K. P., Stjern, C. W., Takemura, T., Voulgarakis, A., and Zwiers, F.: PDRMIP: A Precipitation Driver and Response Model Intercomparison Project, Protocol and preliminary results, Bull. Am. Meteorol. Soc., 98, 1185–1198, https://doi.org/10.1175/bams-d-16-0019.1, 2016.

Myhre, G., Shindell, D., Bréon, F.-M., Collins, W., Fuglestvedt, J., Huang, J., Koch, D., Lamarque, J.-F., Lee, D., Mendoza, B., Nakajima, T., Robock, A., Stephens, G., Takemura, T., and Zhang, H.: Anthropogenic and Natural Radiative Forcing, in: Climate Change 2013: The Physical Science Basis. Contribution of Working Group I to the Fifth Assessment Report of the Intergovernmental Panel on Climate Change, edited by: Stocker, T. F., Qin, D., Plattner, G.-K., Tignor, M., Allen, S. K., Boschung, J., Nauels, A., Xia, Y., Bex, V., and Midgley, P. M., Cambridge University Press, Cambridge, United Kingdom and New York, NY, USA, 659–740, https://doi.org/10.1017/cbo9781107415324.018, 2013.

Penner, J. E., Andreae, M., Annegarn, H., Barrie, L., Feichter, J., Hegg, D., Jayaraman, A., Leaitch, R., Murphy, D., Nganga, J., and Pitari, G.: Aerosols, their Direct and Indirect Effects, in: Climate Change 2001: The Scientific Basis. Contribution of Working Group I to the Third Assessment Report of the Intergovernmental Panel on Climate Change, edited by: Houghton, J. T., Ding, Y., Griggs, D. J., Noguer, M., Linden, P. J. van der, Dai, X., Maskell, K., and Johnson, C. A., Cambridge University Press, Cambridge, United Kingdom and New York, NY, USA, 289–348, 2001.

Pincus, R. and Baker, M. B.: Effect of precipitation on the albedo susceptibility of clouds in the marine boundary layer, Nature, 372, 250–252, https://doi.org/10.1038/372250a0, 1994.

https://doi.org/10.5194/egusphere-2026-6647
Preprint. Discussion started: 4 November 2026
© Author(s) 2026. CC BY 4.0 License.

Ramaswamy, V., Boucher, O., Haigh, J., Hauglustaine, D., Haywood, J., Myhre, G., Nakajima, T., Shi, G. Y., and Solomon, S.: Radiative forcing of climate change, in: Climate Change 2001: The Scientific Basis. Contribution of Working Group I to the Third Assessment Report of the Intergovernmental Panel on Climate Change, edited by: Houghton, J. T., Ding, Y., Griggs, D. J., Noguer, M., Linden, P. J. van der, Dai, X., Maskell, K., and Johnson, C. A., Cambridge University Press, Cambridge, United Kingdom and New York, NY, USA, 349–416, 2001.

Rotstayn, L. D. and Liu, Y.: A smaller global estimate of the second indirect aerosol effect, Geophys. Res. Lett., 32, https://doi.org/10.1029/2004gl021922, 2005.

Rotstayn, L. D. and Penner, J. E.: Indirect Aerosol Forcing, Quasi Forcing, and Climate Response, J. Clim., 14, 2960–2975, https://doi.org/10.1175/1520-0442(2001)014<2960:iafqfa>2.0.co;2, 2001.

Smith, C. J., Kramer, R. J., Myhre, G., Alterskjær, K., Collins, W., Sima, A., Boucher, O., Dufresne, J.-L., Nabat, P., Michou, M., Yukimoto, S., Cole, J., Paynter, D., Shiogama, H., O'Connor, F. M., Robertson, E., Wiltshire, A., Andrews, T., Hannay, C., Miller, R., Nazarenko, L., Kirkevåg, A., Olivié, D., Fiedler, S., Lewinschal, A., Mackallah, C., Dix, M., Pincus, R., and Forster, P. M.: Effective radiative forcing and adjustments in CMIP6 models, Atmos. Chem. Phys., 20, 9591–9618, https://doi.org/10.5194/acp-20-9591-2020, 2020a.

Smith, C. J., Kramer, R. J., Myhre, G., Forster, P. M., Soden, B. J., Andrews, T., Boucher, O., Faluvegi, G., Fläschner, D., Hodnebrog, Ø., Kasoar, M., Kharin, V., Kirkevåg, A., Lamarque, J. -F., Mülmenstädt, J., Olivié, D., Richardson, T., Samset, B. H., Shindell, D., Stier, P., Takemura, T., Voulgarakis, A., and Watson-Parris, D.: Understanding Rapid Adjustments to Diverse Forcing Agents, Geophys. Res. Lett., 45, 12,023-12,031, https://doi.org/10.1029/2018gl079826, 2018.

Smith, C. J., Kramer, R. J., and Sima, A.: The HadGEM3-GA7.1 radiative kernel: the importance of a well-resolved stratosphere, Earth Syst. Sci. Data, 12, 2157–2168, https://doi.org/10.5194/essd-12-2157-2020, 2020b.

Soden, B. J., Broccoli, A. J., and Hemler, R. S.: On the Use of Cloud Forcing to Estimate Cloud Feedback, J. Clim., 17, 3661–3665, https://doi.org/10.1175/1520-0442(2004)017<3661:otuocf>2.0.co;2, 2004.

Soden, B. J., Held, I. M., Colman, R., Shell, K. M., Kiehl, J. T., and Shields, C. A.: Quantifying Climate Feedbacks Using Radiative Kernels, J. Clim., 21, 3504–3520, https://doi.org/10.1175/2007jcli2110.1, 2008.

Taylor, K. E., Crucifix, M., Braconnot, P., Hewitt, C. D., Doutriaux, C., Broccoli, A. J., Mitchell, J. F. B., and Webb, M. J.: Estimating Shortwave Radiative Forcing and Response in Climate Models, J. Clim., 20, 2530–2543, https://doi.org/10.1175/jcli4143.1, 2007.

Toll, V., Christensen, M., Quaas, J., and Bellouin, N.: Weak average liquid-cloud-water response to anthropogenic aerosols, Nature, 572, 51–55, https://doi.org/10.1038/s41586-019-1423-9, 2019.

https://doi.org/10.5194/egusphere-2026-6647
Preprint. Discussion started: 4 November 2026
© Author(s) 2026. CC BY 4.0 License.

Twomey, S.: The Influence of Pollution on the Shortwave Albedo of Clouds, J. Atmos. Sci., 34, 1149–1152, https://doi.org/10.1175/1520-0469(1977)034<1149:tiopot>2.0.co;2, 1977.

Vial, J., Dufresne, J.-L., and Bony, S.: On the interpretation of inter-model spread in CMIP5 climate sensitivity estimates, Clim. Dyn., 41, 3339–3362, https://doi.org/10.1007/s00382-013-1725-9, 2013.

Wang, S., Wang, Q., and Feingold, G.: Turbulence, Condensation, and Liquid Water Transport in Numerically Simulated Nonprecipitating Stratocumulus Clouds, J. Atmos. Sci, 60, 262–278, https://doi.org/10.1175/1520-0469(2003)060<0262:TCALWT>2.0.CO;2, 2003.

Xue, H. and Feingold, G.: Large-Eddy Simulations of Trade Wind Cumuli: Investigation of Aerosol Indirect Effects, J. Atmos. Sci., 63, 1605–1622, https://doi.org/10.1175/JAS3706.1, 2006.

Zelinka, M. D., Andrews, T., Forster, P. M., and Taylor, K. E.: Quantifying components of aerosol-cloud-radiation interactions in climate models, J. Geophys. Res.: Atmos., 119, 7599–7615, https://doi.org/10.1002/2014jd021710, 2014.

Zelinka, M. D., Klein, S. A., and Hartmann, D. L.: Computing and Partitioning Cloud Feedbacks Using Cloud Property Histograms. Part I: Cloud Radiative Kernels, J. Clim., 25, 3715–3735, https://doi.org/10.1175/jcli-d-11-00248.1, 2012.

Zelinka, M. D., Smith, C. J., Qin, Y., and Taylor, K. E.: Comparison of methods to estimate aerosol effective radiative forcings in climate models, Atmos. Chem. Phys., 23, 8879–8898, https://doi.org/10.5194/acp-23-8879-2023, 2023.

Zhang, J. and Feingold, G.: Distinct regional meteorological influences on low-cloud albedo susceptibility over global marine stratocumulus regions, Atmos. Chem. Phys., 23, 1073–1090, https://doi.org/10.5194/acp-23-1073-2023, 2023.

Zhao, M., Golaz, J. -C., Held, I. M., Guo, H., Balaji, V., Benson, R., Chen, J. -H., Chen, X., Donner, L. J., Dunne, J. P., Dunne, K., Durachta, J., Fan, S. -M., Freidenreich, S. M., Garner, S. T., Ginoux, P., Harris, L. M., Horowitz, L. W., Krasting, J. P., Langenhorst, A. R., Liang, Z., Lin, P., Lin, S. -J., Malyshev, S. L., Mason, E., Milly, P. C. D., Ming, Y., Naik, V., Paulot, F., Paynter, D., Phillipps, P., Radhakrishnan, A., Ramaswamy, V., Robinson, T., Schwarzkopf, D., Seman, C. J., Shevliakova, E., Shen, Z., Shin, H., Silvers, L. G., Wilson, J. R., Winton, M., Wittenberg, A. T., Wyman, B., and Xiang, B.: The GFDL Global Atmosphere and Land Model AM4.0/LM4.0: 1. Simulation Characteristics With Prescribed SSTs, J. Adv. Model. Earth Syst., 10, 691–734, https://doi.org/10.1002/2017ms001208, 2018a.

Zhao, M., Golaz, J. -C., Held, I. M., Guo, H., Balaji, V., Benson, R., Chen, J. -H., Chen, X., Donner, L. J., Dunne, J. P., Dunne, K., Durachta, J., Fan, S. -M., Freidenreich, S. M., Garner, S. T., Ginoux, P., Harris, L. M., Horowitz, L. W., Krasting, J. P., Langenhorst, A. R., Liang, Z., Lin, P., Lin, S. -J., Malyshev, S. L., Mason, E., Milly, P. C. D., Ming, Y., Naik, V., Paulot, F., Paynter, D., Phillipps, P., Radhakrishnan, A., Ramaswamy, V., Robinson, T., Schwarzkopf, D., Seman, C. J., Shevliakova, E., Shen, Z., Shin, H., Silvers, L. G., Wilson, J. R., Winton, M., Wittenberg, A. T., Wyman, B., and Xiang, B.: The GFDL Global Atmosphere and Land Model AM4.0/LM4.0: 2. Model Description, Sensitivity Studies, and Tuning Strategies, J. Adv. Model. Earth Syst., 10, 735–769, https://doi.org/10.1002/2017ms001209, 2018b.